PERU FORE-ARC SEDIMENTATION: SeaMARC II
SIDE-SCAN INTERPRETATION OF AN ACTIVE CONTINENTAL MARGIN

A THESIS SUBMITTED TO THE GRADUATE DIVISION OF THE
UNIVERSITY OF HAWAII IN PARTIAL FULFILLMENT
OF THE REQUIREMENTS FOR THE DEGREE OF

MASTER OF SCIENCE

IN MARINE GEOLOGY & GEOPHYSICS

AUGUST 1987

By

Wade Allen Bartlett

Thesis Committee:

Donald M. Hussong, Chairman
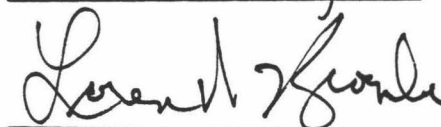Gerard J. Fryer
Loren W. Kroenke

We certify that we have read this thesis and that, in our opinion, it is satisfactory in scope and quality as a thesis for the degree of Master of Science in Marine Geology & Geophysics.

THESIS COMMITTEE

_____
Chairman

_____
Gerard J. Fryer

_____

ACKNOWLEDGEMENTS

Acknowledgements for this thesis include my committee members Don M. Hussong, chairman, Gerard J. Fryer, and Loren W. Kroenke for their comments and editing. Special thanks to Don for his help in starting me, however painful, on this road of side-scan sonar imagery research.

For their editing of preliminary drafts I would like to express my thanks to Fred Duennebier and Bill Coulbourn.

I would also like to thank Kathy for staying with me through this ordeal and giving me support and love when I needed it.

Last I would like to recognize the fellow graduates who were there for support, Bob Mallonee, Bob Lauritzen, Bruce Wedgeworth, Mike Knight, Sylvia Newsom, and Lisa Morzel.

TABLE OF CONTENTS

TABLE OF CONTENTS (cont.)

LIST OF TABLES

LIST OF ILLUSTRATIONS

LIST OF ILLUSTRATIONS (cont.)

Chapter I

Introduction

Previous studies of sediment transport on continental margins have concentrated on submarine canyons and turbidite fan systems, largely on stable continental margins. Comparatively little attention has been directed toward the relatively unstable geomorphology of active subducting continental margins. Most of these previous studies have also been based on trackline surveys which require interpolation of data between ship's tracks, thereby showing large seafloor features but often missing important subtle features. Newly available swath-mapping techniques, eg. SeaMARC II (Sea Mapping and Remote Characterization), are now capable of providing continuous coverage of large areas. Recently, the submarine active continental margin off central Peru (Figure 1) was surveyed using the SeaMARC II side-scan sonar imagery and bathymetric swath-mapping system, revealing a variety of subtle sediment features [Hussong et al., 1985]. The purpose of this paper is to interpret these same sediment morphological features and to determine the causes for their formation and distribution.

Sediment features on the active continental margin of Peru are more intricate than expected. The ubiquitous hemipelagic sediments which completely blanket most continental margins are eroding and redepositing in select areas to form complicated underwater "drainage patterns". The nature, causes, and consequences of this sediment
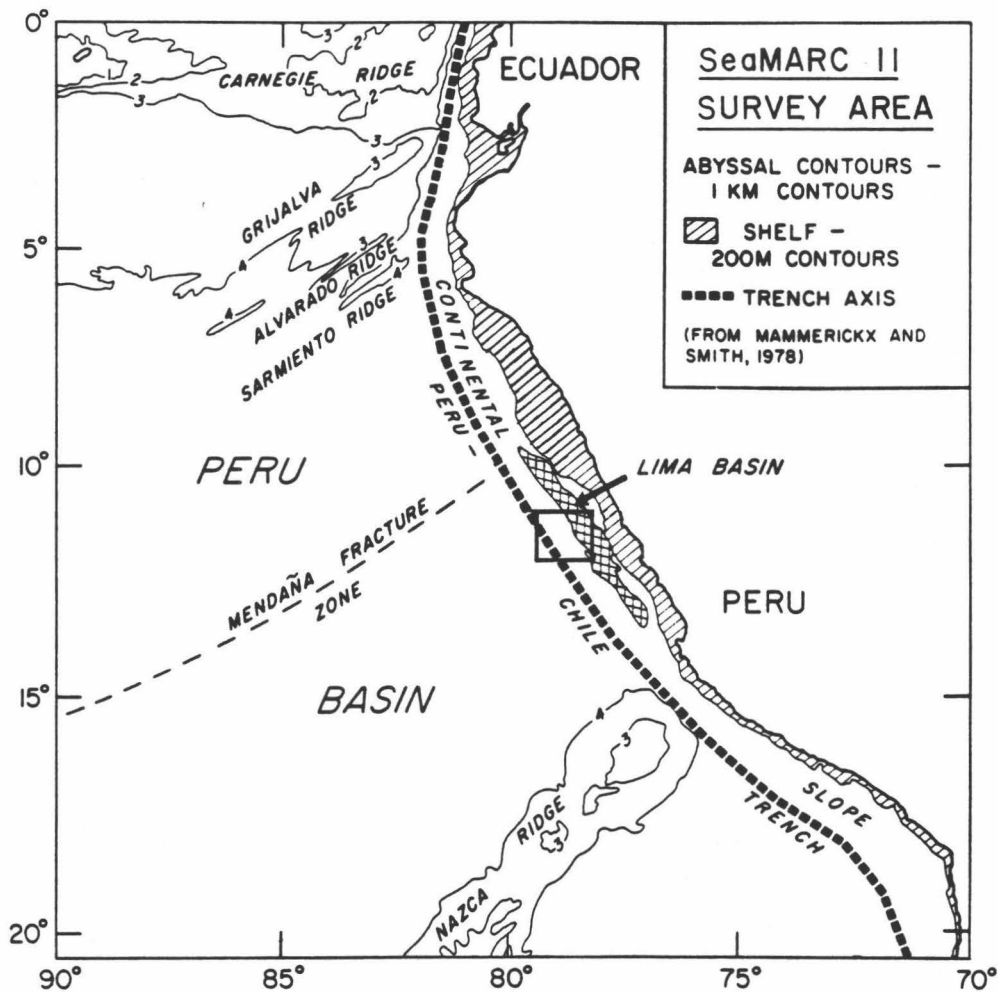
Fig. 1. Study area location showing SeaMARC II side-scan sonar and bathymetry swath mapping coverage. Note the relationship of the study area to the extent of Lima Basin upper-slope basin (reticulated pattern) and with respect to the Mendana Fracture Zone.

transport are responsible for most of the seafloor morphology of the central Peru fore-arc.

The Peru convergent continental margin has been an area of extensive research for the last 15 years. It has been described as a type end-member of convergent margins where oceanic lithosphere subducts under purely continental lithosphere in an uncomplicated fashion [Barazangi and Isacks, 1976]. The Nazca Plate Project, a comprehensive study of the continental margin and associated oceanic plates, was undertaken during the early 1970's in an effort to understand the interaction between a total oceanic plate that is fairly small, but mature and stable, and an active continental margin that is uncomplicated by back-arc spreading, aseismic ridge or seamount subduction, migrating triple junctions along the trench, or allochthonous terrains. Much of this work is summarized in two volumes, Sutton et al., [1976] and Kulm et al. [1981a].

In 1985 the Peru margin was revisited as part of a scientific drilling target selection site survey for the Ocean Drilling Program. This survey included extensive coverage by SeaMARC II side-scan sonar and swath bathymetry mapping, multichannel seismic reflection profiling, and bottom sampling (Figure 2). This paper is concerned primarily with interpretation of the SeaMARC II data.
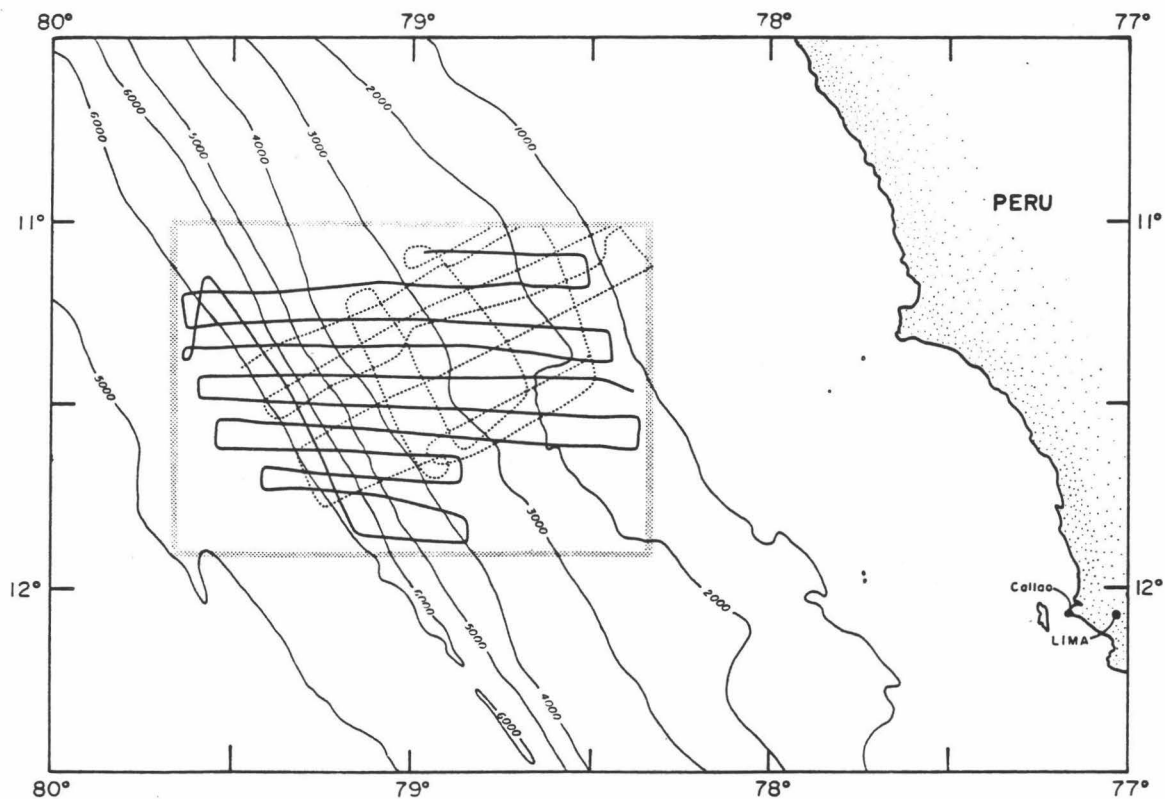
Fig. 2. SeaMARC II and multichannel seismic trackline coverage in the Lima Basin survey area. Solid lines represent the SeaMARC II and single channel seismic coverage (oblique to structure) and the dashed lines designate the multichannel lines (perpendicular and parallel to structure). All lines have 3.5 kHz data.

Chapter II

Geologic and Tectonic History

Fore-arc

Lima Basin. The Lima Basin is defined by Thornburg and Kulm
[1981] as an upper-slope basin. It extends from 10°S to 14°S latitude
and is confined between two sub-basement structural ridges that have
been seismically mapped by Thornburg and Kulm [1981] and named the
Outer Shelf High (OSH) on the landward side and the Upper Slope Ridge
(USR) on the seaward side (Figure 3). These two ridges were important
structural highs in the early history of the formation of the Basin.
It is uncertain as to whether the USR was a center of volcanism at the
Mesozoic onset of subduction [Marocco, 1981], or uplifted when the
continent was tectonically eroded back to the USR. Regardless of its
early history, the USR has likely remained an effective confining
structure for the collection of sediments in the Lima Basin in much of
the Cenozoic.

The OSH was a center of subduction-related volcanism in the early
history of this margin before the volcanism moved east to the area of
the Peru coastal batholiths. The exact timing of emplacement of the
OSH is a matter of conjecture. This eastward migration in the age of
the volcanics is observed in the linear volcanic belts trending
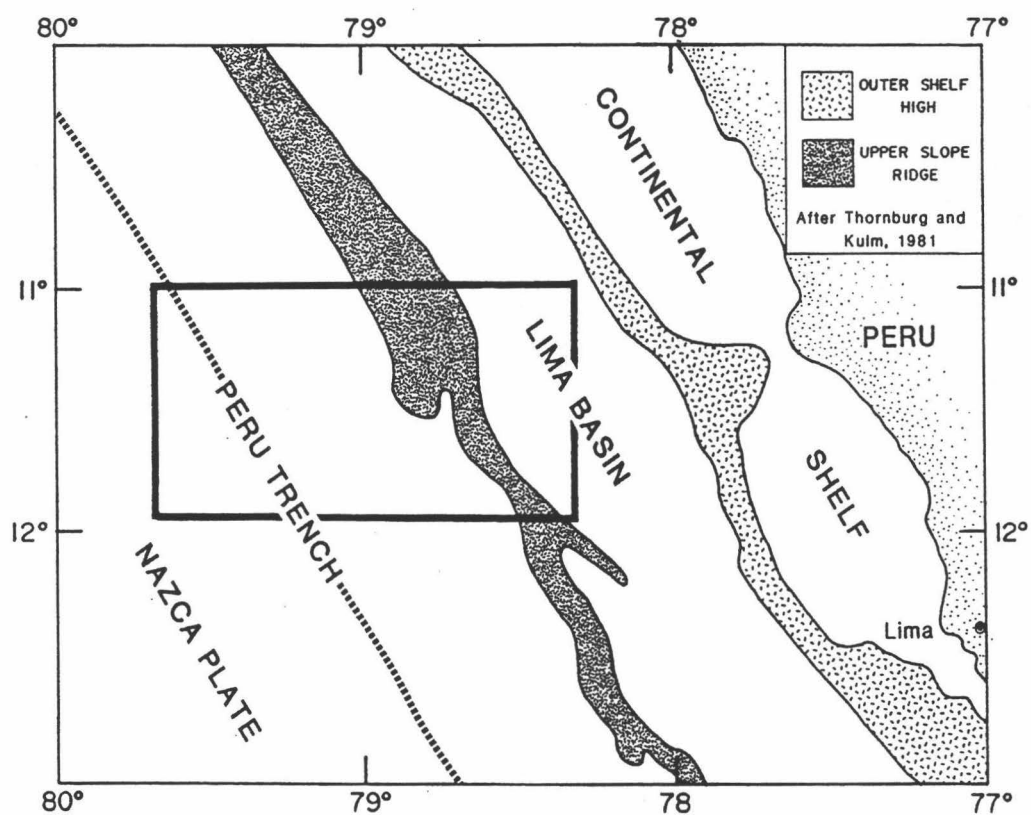
Fig. 3. Map showing major structual highs at the surface and subsurface that define Lima Basin on the upper-slope of the Peru continental margin.

parallel to the trench axis and Peru coastline [Masias, 1976; Thorpe and Francis, 1979].

Lima Basin Section. In general, the Lima Basin is composed of consolidated, hemipelagic sediments overlying metamorphic continental basement. A thin veneer of the most recent unconsolidated hemipelagic sediments covers some parts of the Basin.

Kulm et al. [1981b] compiled a section of the Lima Basin based on dredges of outcrops in the walls of various submarine canyons at different depths on the upper slope. The top 700 m of this section is comprised of hemipelagic mud, dolomicrite with interbedded calcareous siltstone, and siltstone of the Pleistocene epoch. Below this lies another 400 m of Pliocene micrite, dolomicrite, brecciated dolomicrite, calcareous siltstone, and siltstone. The deepest 900 m of the section is upper Miocene dolomicrites and brecciated dolomicrites. Acoustic basement is assumed to be crystalline metamorphic rock, based on samples from commercial wells drilled farther north in the Yaquina Basin [Kulm et al., 1981b; Kulm et al., 1982; von Huene et al., 1985].

The hemipelagic sediments which form a thin and often irregular blanket over the fore-arc have been subject to considerable lateral transport. The main source of these sediments is the prominent coastal up-welling that form large depth restricted mud lenses on the continental shelf [Schweller and Kulm, 1978; Krissek et al., 1980; Busch and Keller, 1983]. The sediment is composed of mud, silt, and sand, and lacks the coarse components typical of a continental shelf dominated by terrestrial stream output [Krissek et al. 1980]. This lack of terrestrial sediment is due to the extreme aridity of the

adjacent Peruvian coastline. What terrestrial input is deposited, is aerially distributed by prevailing southeasterly trades [Johnson, 1976; Krissek et al., 1980; Busch and Keller, 1981; Busch and Keller, 1982]. This fine-grained terrigenous input gives a dark gray-green appearance to the hemipelagic sediment observed in cores.

A large portion of the sediment fill in the trench comes from the north where more rivers empty into the ocean [Krissek et al., 1980].

Subsidence. Kulm et al. [1981b], using benthic faunas in dredged carbonate rocks, suggest 500 m of subsidence of the landward flank of Lima Basin over the past 1.0 m.y. and 1100 m of subsidence of upper Miocene to Pliocene carbonates in the seaward flank of the Basin. Assuming the interpretations of Hussong et al., [1976], Kulm et al., [1981b], and von Huene et al., [1985], that the basement rock is crystalline metamorphic continental rock, then this vertical tectonic motion involves movement of the sub-Andean continent. Adjustments to the geometry of the subducting oceanic lithosphere and the thickness of the continental fore-arc may cause the fore-arc to subside in a regional fashion.

Geometry of Sedimentation. Coulbourn and Moberly [1977] plotted two-way travel time between reflectors observed in single channel records in the Iquique and Arica fore-arc basins, south of this survey area. They show a progressive, although irregular, eastward shift of the axis of maximum sedimentation due to landward tilting of the basins through time. Their interpretation of the cause of this rotation was either an uplift of a structual high on the outer fore-arc, compaction due to overburden weight, or downthrow along the seaward side of faults

paralleling the coastline. Single-channel seismic profiles in the Lima Basin demonstrate similiar differential vertical tectonic motion.

Tectonics

Forces on the Subducting Plate. The Nazca Plate bends as it subducts, causing extension to the top of the oceanic lithosphere, and typical pre-subduction normal faulting [Hussong et al., 1976; Searle et al., 1981]. At the trench and after initial subduction the Nazca plate may then be subject to compressive forces as it unbends into a straight Benioff zone [Hussong and Wipperman, 1981]. Compressive forces would also result from the upper oceanic crust locking against the continental margin [James, 1978; Schweller et al., 1981]. In either situation the straightening would cause the upper-part of the plate to be in compression.

Accretion vs. Subduction. There has been considerable disagreement as to whether the Peru margin is accreting or is being tectonically eroded. Critical to this discussion is the size and nature of the accretionary wedge. In this survey area the accretionary wedge is relatively small.

The accretionary wedge is interpreted as the 4 km/sec material in the Hussong and Wipperman [1981] velocity model derived from the CDP-1 reflection seismic profile across the trench, Lima Basin and continental margin. This low velocity wedge extends 15 km from the trench axis into the landward wall. If a minimum 100 m years of subduction have occurred along this plate margin [Hussong et al., 1976; Kulm et al., 1977], and the order of 200 m of sediment on the oceanic plate are carried into the trench, only a small fraction (less than

10%) of that sediment now exists in the form of an accretionary wedge. The onset of subduction may even extend to 150 m.y. [Hussong et al., 1976] making the small size of the accretionary wedge even more perplexing.

If sediment has been subducted with the slab, its appearance in the chemical signature found in the erupted lavas on Peru is not clear. Much of this uncertainity occurs because there has been a lack of recent volcanism between 2° and 14° S across Peru. However, the chemical data are ambiguous because of possible contamination of the melt by the overlying mantle wedge and or the thick continental lithosphere through which the magma must ascend [Pearce, 1982; Hawkesworth, 1982]. Thus although data from Peru is not conclusive, most evidence points to little contribution from the subducted sediments in the chemical signature of erupted lavas in Peru.

Nevertheless, the lack of sediment in the form of an accretionary wedge suggests subduction of the sediment with the downgoing oceanic lithosphere. Hilde and Sharman [1978] have suggested that sediment may be trapped and subducted in grabens forming due to the extensional forces imposed on the plate as it bends to subduct. Subducting grabens on the Peru margin have been detected in multichannel records [Hussong and Wipperman, 1981] and in GLORIA reconnaissance side-scan data [Searle et al., 1981].

If accretion has occurred, one candidate mechanism is underplating of the overriding slab. Hussong et al. [1976] and Hussong and Wipperman [1981] discuss the further possibility of underthrusting of

the subducting oceanic crust beneath itself; essentially resulting in underplating of both oceanic sediments and crust. Obviously not all the sediments have been underplated; some quantities must be subducted. Periods of accretion may alternate with periods of tectonic erosion. How underplating of buoyant sediments affects the vertical tectonics of the continental margin is not clear, but during periods of accretion, the continental margin must be built upward and outward and during tectonic erosion, the margin must be truncated and sediment removed with the subducting lithosphere.

Chapter III

Methods

A marine geophysical investigation of the Peru continental margin and trench between 11° and 12° S was carried out during three consecutive legs of the R/V MOANA WAVE between February 28 and April 17, 1985. Data collected during these legs include: SeaMARC II side-scan sonar and swath bathymetry data with single channel seismics (generally a 40 cubic inch airgun source, 40-100/100-300 Hz frequency) and 3.5 kHz sub-bottom profiler data, (MW8504; Figure 2); multichannel 24-fold data with 3.5 kHz data (MW8505; Figure 2); and rock dredge, piston, gravity, and rock core data (MW8506).

The SeaMARC II side-scan sonar imaging and bathymetric mapping system was the principle source of data used in this study. The SeaMARC II system and the data interpretation techniques used in this study are described below.

SeaMARC II Description

SeaMARC II is a long-range, high-resolution, side-scan sonar system with the unique capability of simultaneously measuring precise bathymetry of the ensonified seafloor. The system employs a transducer array that is towed at a shallow depth, typically 100 m below the sea surface, where it is isolated from surface waves and is below the strong sound-speed gradients found near the surface. The system

operates at 11 kHz on the port side and 12 kHz on the starboard side. For a more complete system description see Blackinton et al. [1983], Hussong and Fryer [1983]. Blackinton [1986] has compiled a historical look at the development of SeaMARC and a comparison of it with other systems.

At seafloor depths greater than 1 km the system is generally configured to produce side-scan images 10 km wide (all data used in this study are in 10 km swaths). At a towed speed of 7 to 8 knots, the 10,000 square km study area of the Lima Basin was ensonified in four days (Figure 4).

The SeaMARC II side-scan images contain 1024 pixels in each half of the swath. The pixel locations are corrected to remove slant range distortion and to account for variations in ships' speed, and then assembled as a mosaic to produce a geometrically correct plan view of the bottom. For a 10 km swath each pixel represents the echo strength from a band 5 m wide across track. The along-track beam width of the towed transducer array is 2° [Hussong and Fryer, 1983].

SeaMARC II sonar signals have a wavelength in water of about 12.5 to 13.5 cm, so the side-scan image is particularly sensitive to reflectivity changes caused by backscatter from seafloor relief on the order of 10 cm. Recognition of seafloor patterns, however, is a function of the type of feature causing the echoes [Hussong and Fryer, 1983]. Typically, linear features such as channels or faults are recognizable if they have dimensions of only a few to several tens of meters.

14

Plate I. SeaMARC II bathymetry of the Lima Basin mosaic. Contour interval is 100 m. The bathymetry does not depict any major canyon system that leads to the trench.

Fig. 4. SeaMARC II side-scan mosaic of the Lima Basin survey area.

PLATE I

79°40'W
11°00'S

78°20'W
11°00'S

11°55'S
79°40'W

11°55'S
78°20'W

16

10 KM
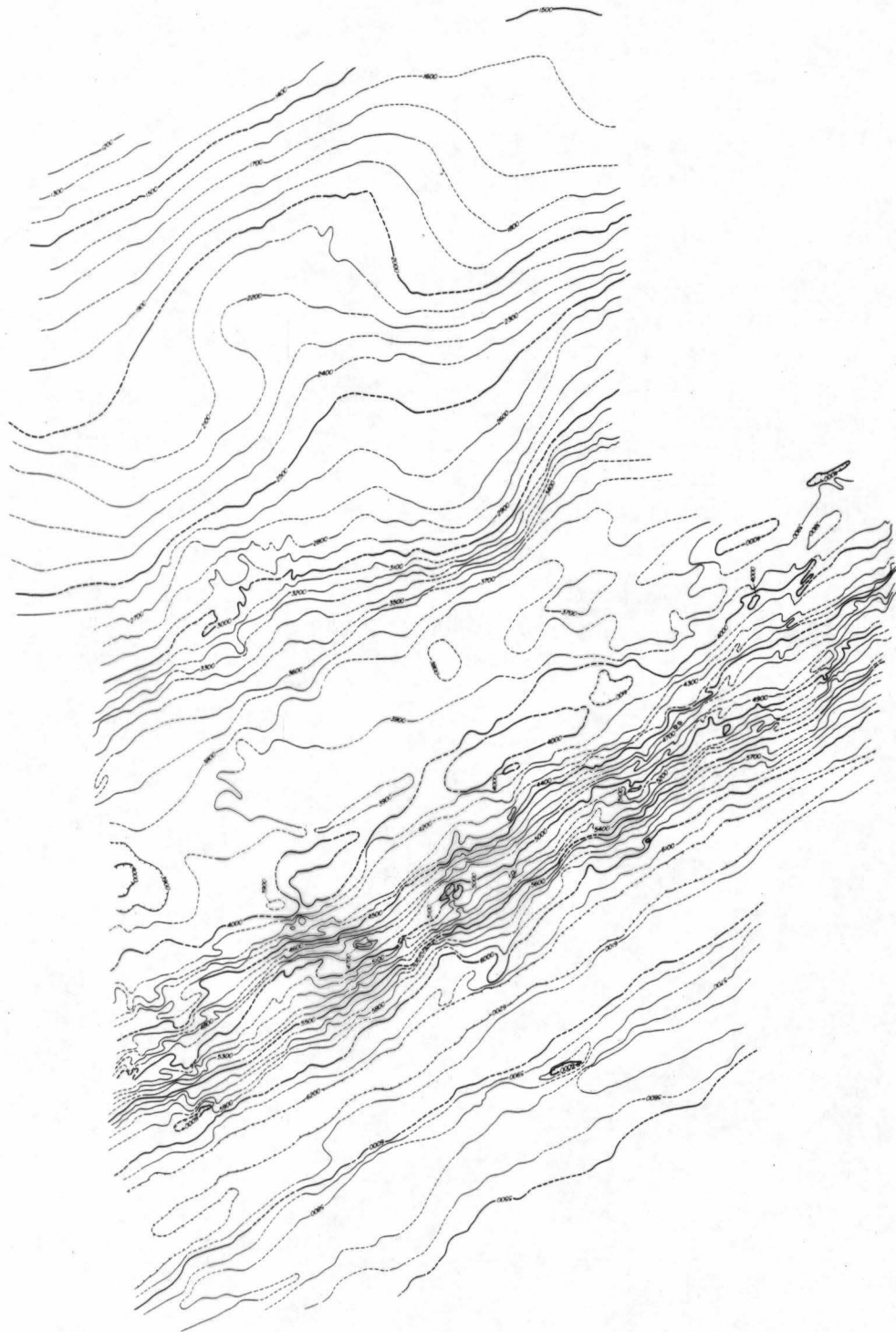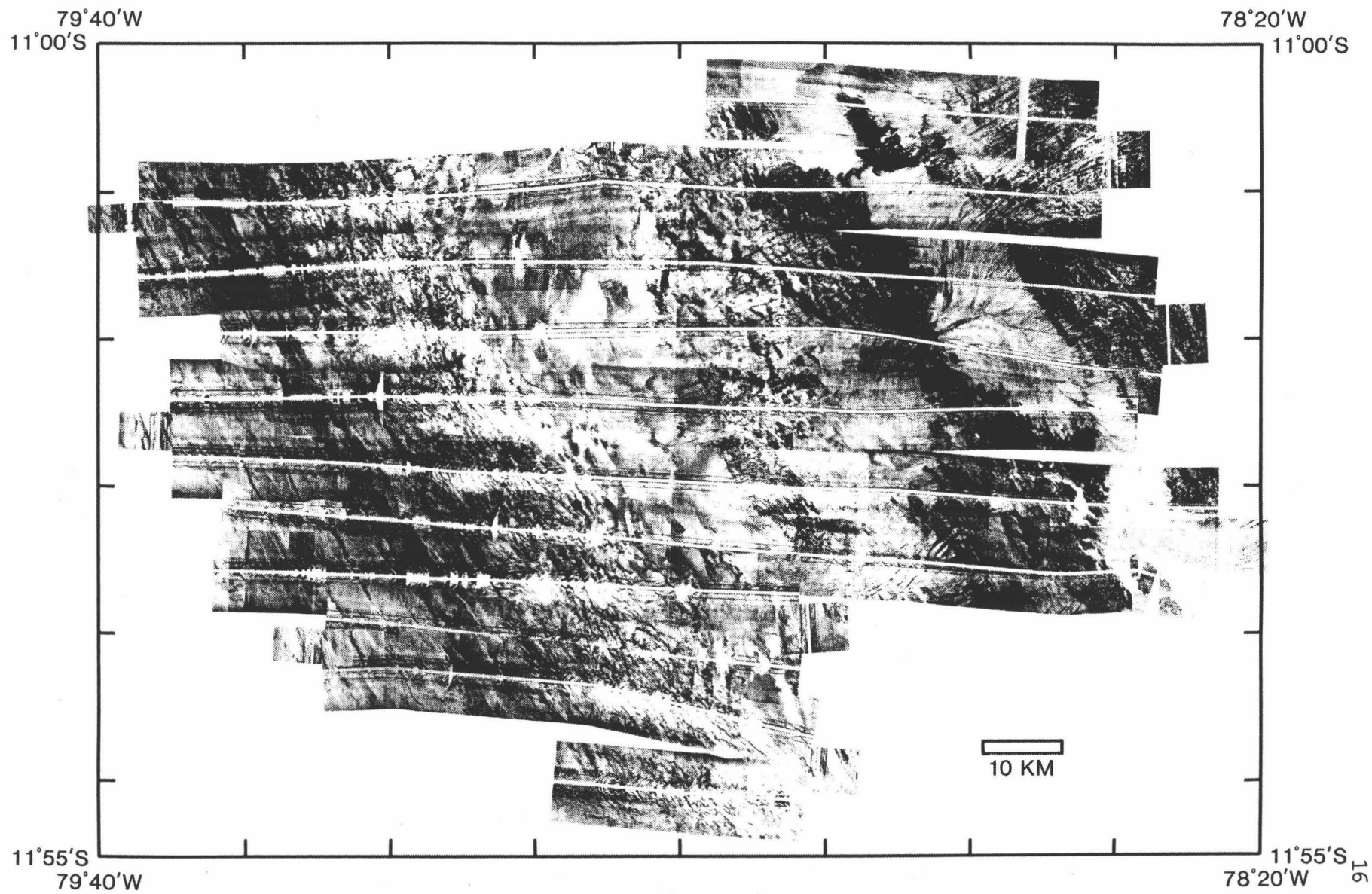
It should be noted that SeaMARC imagery differs from both standard remote-sensing and other side-scan systems by reversing the polarity of the amplitude data. In SeaMARC II images low-amplitude echoes such as from sediments and flat lying specular surfaces, are printed in light grays (see specular vs. back-scattering below). High-intensity return areas such as slopes, rough surfaces, and outcrops, are printed darker grays to black. Thus, acoustic shadows appear as white on SeaMARC mosaics. Since the ocean bottom is dominated by large areas of sediment and few strong reflectors, this system of reversing the amplitude keeps the important features enhanced and allows distinguishing features to be more readily recognized.

Processing SeaMARC II Data. The processing and preparation of a mosaic of the SeaMARC II side-scan data used in this study was performed at sea. Corrections due to ship's speed and to pixel location errors caused by inaccurate bottom depth detection were accomplished within a day of the completion of smoothed shipboard navigation. Navigation was based on Transit satellite, with position interpolation corrected using calculated set and drift. Navigational accuracy is typically better than 1 km. Corrected side-scan was plotted in strips on a dot matrix plotter and assembled into a spatially correct picture, called a mosaic.

Processing on board the ship enabled a side-scan mosaic to be used for the subsequent multichannel seismic profiling and bottom sampling legs.

Bathymetric data were processed when the digitized tapes were returned to Hawaii Institute of Geophysics. In addition to the routine

processing, some image processing of the side-scan was completed post-cruise. This included beam pattern corrections to enhance low-amplitude data and to suppress near-nadir high-intensity specular returns along and across the ship's track, essentially correcting problems with system gain changes [Reed, 1987]. This processing aids the overall appearance of the data set, and makes subtle features in sedimented areas more identifiable. Reed [1987] has accumulated systematic processing routines for quantitative image enhancement of side-scan sonar data, specifically SeaMARC II.

Techniques for Interpretation of Side-scan

Side-scan sonar is used here as a geological mapping tool for an "aerial view" of the ocean bottom using sound instead of light. The physical properties that create the side-scan is important for the interpretation of subtle sediment features.

A few side-scan terms and concepts used in this paper, which may or may not be familiar to the reader are described below. For a more comprehensive discussion of side-scan techniques in general see Trabant [1984, Chapter #6]. For a side-scan sonar users manual for the geologist see Mazel [1985] who describes various aspects and pitfalls of side-scan sonar interpretation.

Specular vs. Back-scattering Surfaces. A specular surface is a mirror surface for which the angles of incidence and reflection are equal (i.e., a surface for which Snell's law is satisfied). In the case of a specular surface most of the energy is reflected away from the receiver and is printed as light shades of gray.

A surface that back-scatters the energy ensonifying it reflects the energy in all directions with some directed back to the receiver. Since some of the energy is reflected directly back toward the receiver the image is printed as darker shades of gray. The surface with intermediate roughness specularly reflects part of the energy and scatters the remainder (Figure 5). This is printed as a gamut of gray level ranges. Backscattering occurs with rougher bottoms and objects that have targets reflecting the energy back to the receiver. The strength of the return is controlled by the height of surface irregularities. This has been quantified in Rayleigh's criterion.

Rayleigh's Criterion: The Rayleigh criterion relates the wavelength of the sonar and look-angle to surface roughness. This criterion is commonly used in radar, but may also be applied to side-scan sonar [T. B. Reed, personal communication, 1986]. The equation below has been modified slightly from Sabins [1978] to account for terminology used in SeaMARC II side-scan sonar studies.

A surface is considered smooth by the Rayleigh criterion if,

$$h < \frac{lambda}{8 \sin(90^{\circ} - \text{look-angle})}$$

where;

h = the height of surface irregularities or surface roughness (cm)

lambda = the sonar wavelength (approximately 13 cm for SeaMARC II)

RECEIVER

LOOK-
ANGLE
$\gamma = 45^0$

ALTITUDE

SeaMARC II
WAVELENGTH
$\lambda = 13$ cm

SPECULARLY REFLECTED WAVE

$h < 0.74$ cm
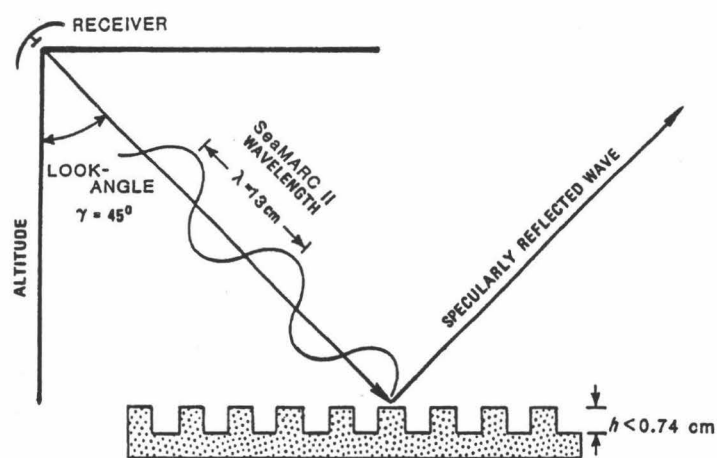
A. SMOOTH SURFACE WITH SPECULAR REFLECTION; NO RETURN.

$h = 0.74$ to 4.18 cm
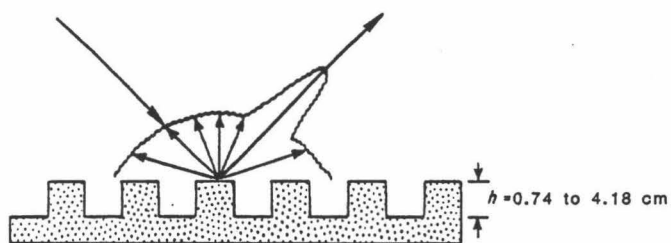
B. INTERMEDIATE SURFACE ROUGHNESS; MODERATE RETURN.

$h = 4.18$ cm
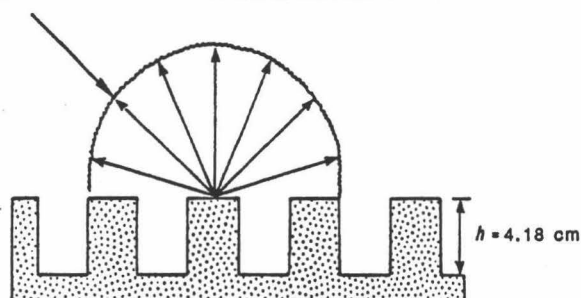
C. ROUGH SURFACE WITH DIFFUSE SCATTERING; STRONG RETURN.

Fig. 5. Models of surface roughness depicting relative return intensity (after Sabins, 1978). The example used represents the SeaMARC II system.

look-angle = the acute angle measured between the vertical
and the incident sonar wave

The limiting value for h, $\dfrac{lambda}{8(\sin \frac{pi}{2} - theta)}$, is the theoretical

boundary between smooth and rough surfaces for the given wavelength and
look-angle. The surface roughness value is a discrete cut-off point
which does not take into consideration the important intermediate
surfaces between definitely smooth and definitely rough. The Rayleigh
criterion was modified by Peake and Oliver [1971] to define the upper
and lower values of h for surfaces of intermediate roughness.

Smooth criterion:

$$h < \frac{lambda}{25 \sin(90^{\circ}- \text{look-angle})} \;.$$

Rough criterion:

$$h > \frac{lambda}{4.4 \sin(90^{\circ}- \text{look-angle})} \;.$$

The relationships of side-scan return intensity to the bottom
surface vertical relief values derived in the preceeding expressions

are illustrated in Figure 5. The relationship between look-angle and surface roughness is shown in Table 1.

Look-Angle. The acute angle from the vertical to a bottom target is called the look-angle. For instance, an angle of 10° would be close to the ship's track and 60° would be near the far edge of the swath away from the ship's track. The grazing angle is the complement of the look-angle and is therefore the acute angle measured from horizontal to the target.

The term nadir is used to refer to the area directly below the towed sonar array (called the "towfish"). This area usually has a high amplitude reflection due to the small look-angle which reflects the energy directly back toward the receiver (Figure 6). This overly dark area is compensated for by gain corrections in post-processing. Anomalous energy returns are symptomatic of variations or changes in seafloor reflectivity and have possible geological implications.

The advantage of towing the SeaMARC II device close to the surface allows steeper look-angles at any water depth. In deeper water the look-angle remains small over the preset 10 km swath width, therefore the energy returned is not affected as much by small relief on the bottom. In shallow water the look-angle becomes larger over the swath and the energy is back-scattered more by small vertical relief. However, the relationship between look-angle and water depth results in the shallow towed SeaMARC II producing images with few shadows from bottom relief.

Table 1. Theoretical surface roughness values of h

for SeaMARC II

(Look-angle vs. Surface Roughness)

look-angle (γ)	smooth h [a]	intermediate	rough h [a]
0°	<0.52	0.52 to 2.95	> 2.95
10°	<0.53	0.53 to 3.00	> 3.00
20°	<0.55	0.55 to 3.14	> 3.14
30°	<0.60	0.60 to 3.41	> 3.41
40°	<0.68	0.68 to 3.86	> 3.86
50°	<0.81	0.81 to 4.60	> 4.60
60°	<1.04	1.04 to 5.91	> 5.91
70°	<1.52	1.52 to 8.64	> 8.64
80°	<3.00	3.00 to 17.01	>17.01

All values are in centimeters.

[a]Values of h from Peake and Oliver [1971] criterion.
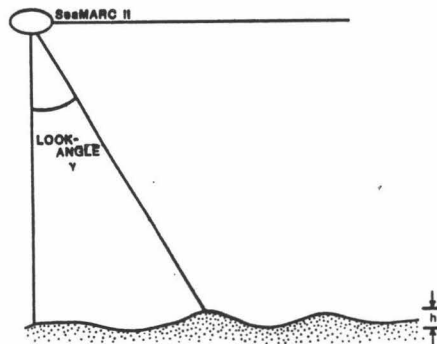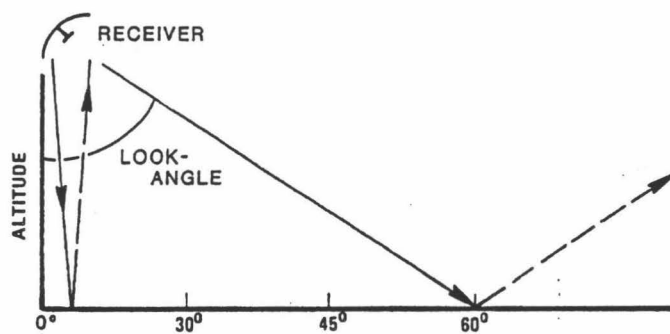
A. SMOOTH SURFACE WITH SPECULAR REFLECTION.
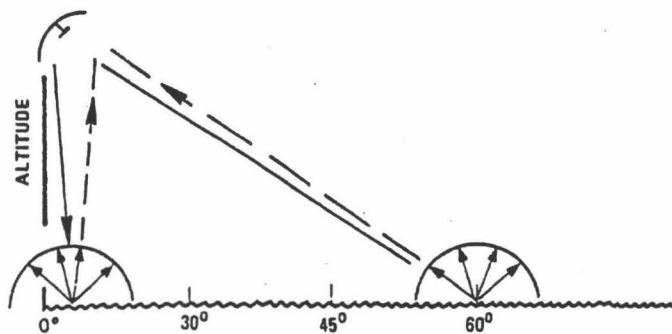
B. ROUGH SURFACE WITH DIFFUSE SCATTERING.
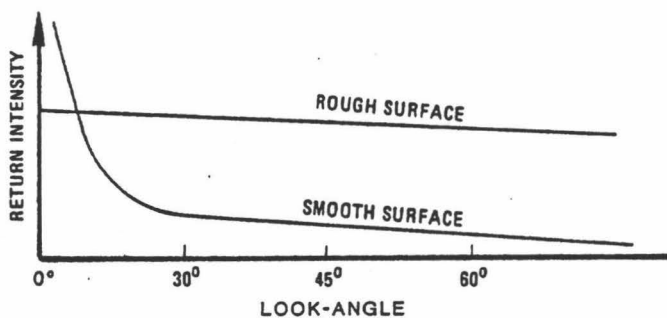
C. RETURN INTENSITY AS A FUNCTION OF LOOK-ANGLE

Fig. 6. Side-scan sonar return from a) a smooth surface and b) a rough surface as a function of the look-angle. c) Shows the theoretical strong return at the point directly below the towfish track (after Sabins, 1978).

Look-Direction. The direction from which the target is ensonified is defined as the look-direction. Depending on the ocean bottom fabric, bottom targets may appear different when viewed from different directions. In the Peru survey tracks were aligned roughly 45° to the regional strike of trench and fore-arc. As we shall see, such an oblique cross direction allows the observer to differentiate between faults and outcrops.

Faults: Surface expressions of faults can be recognized by their distinct character when viewed obliquely by side-scan. The energy that encounters the face of the fault scarp is strongly reflected, and is displayed as a dark set of pixels. When crossed, the fault is ensonified from the upthrown side, so the scarp creates an acoustic shadow on the side-scan image.

If a fault scarp is orientated perpendicular to the ship's track, recognition may be more difficult and depend on the texture of the scarp's face or fault breccia. Oblique dark lines can occasionally be traced through an entire swath, meaning different look directions produced no difference in back-scattered energy. This is observed only at steep look-angles and must result from the rough texture of the scarp. In this case energy is returned fairly symmetrically on both sides and a uniform dark band is printed across the swath. In this special case the geologist must rely on "geological common sense" to determine the nature and throw of possible faults.

Outcrops: The identification of an outcrop based on look-direction is controlled by texture. The surface expression of

outcropping strata is assumed to have lateral homogeneity across track. In this case opposite sides of the records reveal a uniform gray-level that passes across the ship's track.

Chapter IV

Results: Description of the SeaMARC II side-scan mosaic

The Lima Basin mosaic (Figure 4) is conveniently divided into the distinct physiographic areas (Figure 7) identified by Thornburg and Kulm [1981] and Hussong and Taylor [1985], based on the generic terminology of a fore-arc described by Dickinson and Seely [1979].

Hussong and Taylor [1985] divided the Lima Basin mosaic into five primary physiographic areas based on morphology and structure. They suggest that the morphology and structure is controlled by disruption of the overiding plate related to variations in thickness of the fore-arc and changes in subduction geometry. The physiographic areas (Figure 7) are aligned roughly parallel to the Peru trench axis (N 32°W) and the normal faults of the Nazca plate (N 28°W). These areas are used to sub-divide the composite mosaic into separate figures for discussion as follows:

(1)   The upper-slope basin (Lima Basin) is a well-developed structural basin situated between two prominent confining ridges on the continental slope (Figure 1 and 3). The basin begins beyond the mosaic coverage and extends 50 km landward of the trench axis. The water depth increases from less than 1200 m to 2200
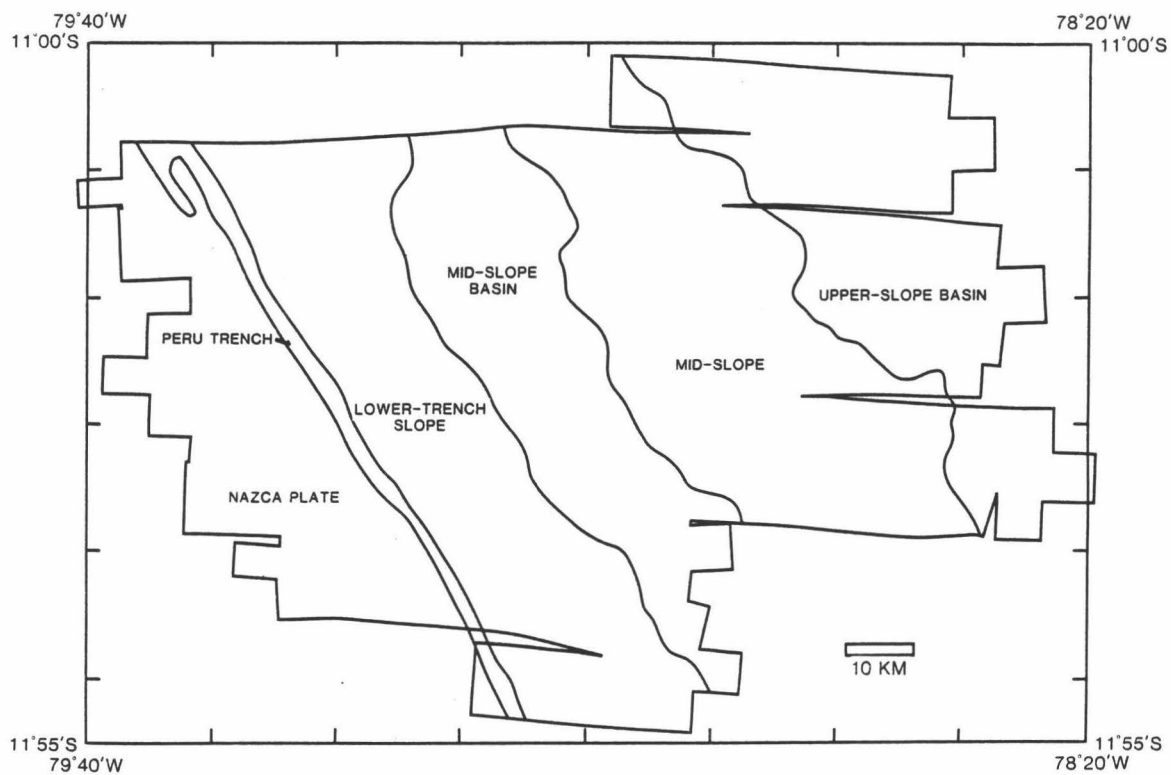
28

Fig. 7. Schematic diagram of the Lima Basin survey area showing the distinctive physiographic areas.

m in the ensonified area. The subducting slab lies at a
depth of 8 km below the seafloor, as interpreted from
multichannel seismic profiles [Hussong and Wipperman,
1981; Hussong and Taylor, 1985].

(2)   The mid-slope is the transition slope between the
upper-slope basin and mid-slope basin, dropping from
depths of 2200 m to 3750 m and is characterized by
disrupted outcropping sedimentary rocks [Kulm et al.,
1981b; Kulm et al., 1985]. This is the proposed
transitional area between the continental massif and
oceanic derived crust [Hussong and Taylor, 1985; Kulm et
al., 1985]. The mid-slope lies between 50 km and 30 km
landward of the trench, with the subducting slab 6 km
below the seafloor [Hussong and Taylor, 1985].

(3)   The mid-slope basin is a well-developed structural
basin extending 30 km landward of the trench to the
trench-slope break (15 km from the trench). Water depth
ranges from 3800 m to 4000 m. The mid-slope basin is
broken into individual pockets interpreted as smaller
independent basins by Hussong and Taylor [1985].

(4)   The lower-slope (inner-trench wall) extends from
the trench-slope break 15 km to the trench-axis and
drops from about 4000 m to greater than 6000 m depth.

This accreted complex is characterized by sediment packets parallel to the trench that have along-strike continuity of tens of kilometers. The slope is steep (from 7° to 9°) and very hummocky, resulting in poor acoustic imaging.

(5)   The trench axis turbidite pond ranges in width from 9 km in the north of the mosaic, where it exists as two turbidite ponds separated by a large thrust ridge [Schweller et al., 1981], to virtually non-existent as it pinches out in the south. Thus in the southern part of the survey area the oceanic plate abuts directly against the accretionary complex. The trench is approximately defined by the 6200 m contour.

Upper-slope basin

A portion of the Lima Basin (Figure 8) identified as the upper-slope basin has been divided into three sub-sections; a northern and southern upper-slope, differentiated according to bathymetric gradients and the degree of normal faulting perpendicular to the trench, and the upper-slope turbidite pond, an oval-shaped accumulation of hemipelagic sediments eroded from those areas (Figure 9).

North
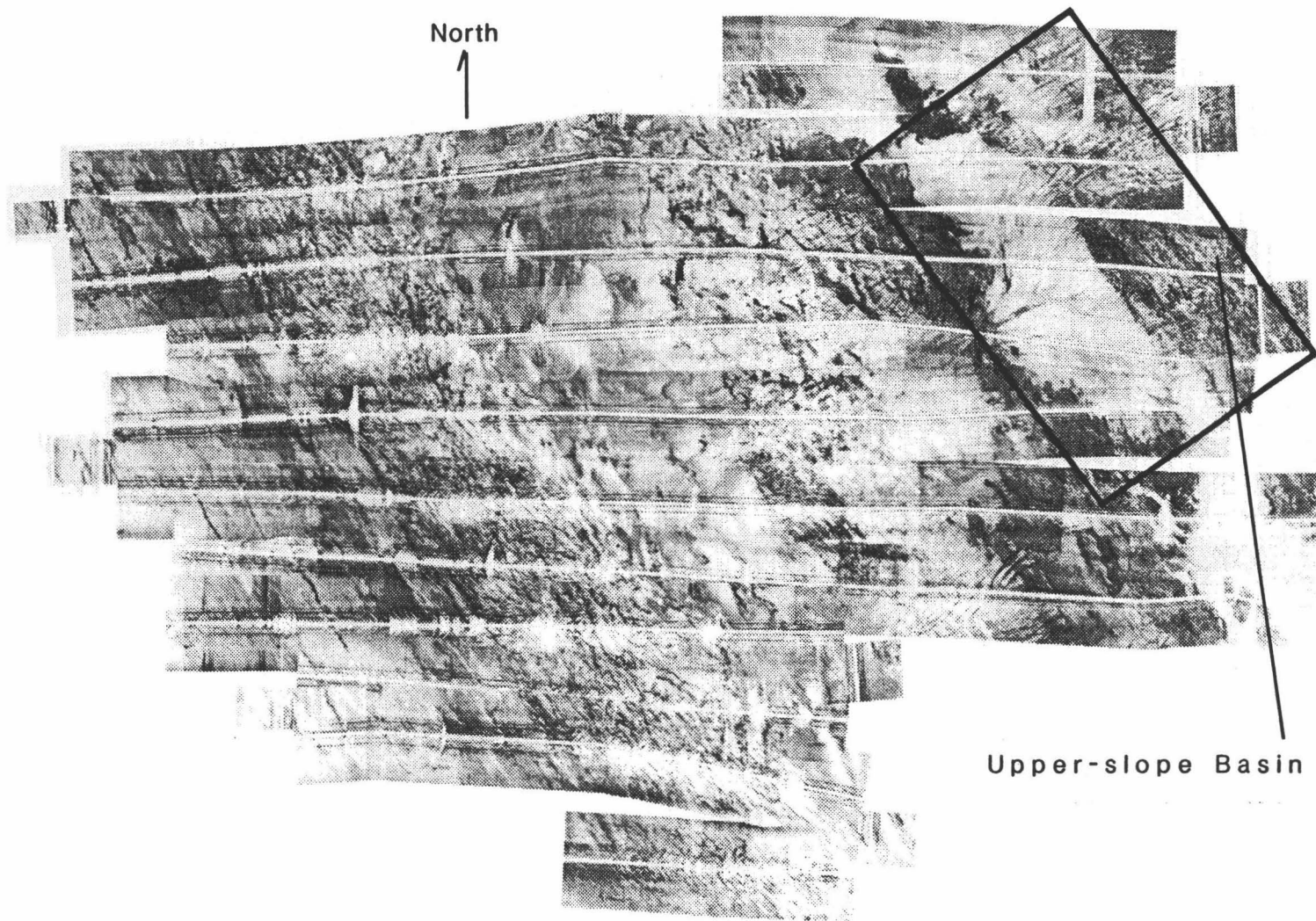
Upper-slope Basin

Fig. 8. The box outlines the location of Figure 9 and 10 relative to the Lima Basin survey mosaic.
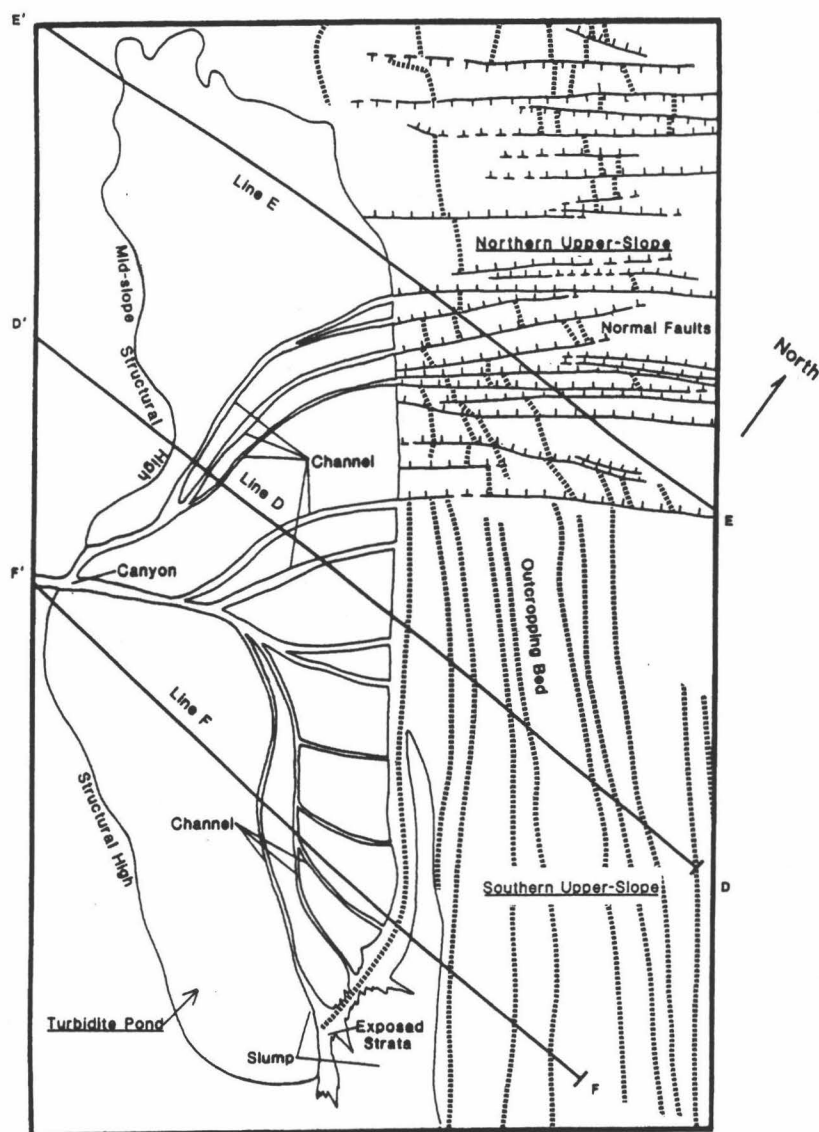
Fig. 9. A simplified interpretation diagram of the side-scan showing locations of the three sub-divisions of the upper-slope: northern upper-slope, southern upper-slope, and upper-slope turbidite pond. Normal faults (horizontal hachured lines) offset outcropping strata (vertical dashed lines) in the northern upper-slope, whereas in the southern upper-slope the outcropping strata are undisturbed. Seismic lines across the region are labeled A - F.

The northern upper-slope has a shallow gradient and a high degree of normal faulting perpendicular to the trench. The southern upper-slope has a steeper gradient, with little disruption due to faulting. The division between these two areas runs perpendicular to the trench and is delineated by the southernmost fault in Figure 9.

The reason for the differences in the slopes between these two adjacent areas is poorly understood, but may be due to subsidence. If the thickness of the fore-arc wedge is 8 km in this area, this may be thin enough to respond to changes in subduction geometry, but thick enough to deform regionally. Local changes in vertical motion would require adjustment that might be expressed as normal faulting. The change in slopes happens abruptly, suggesting that a fault serves as a detachment surface between the areas.

In the northern part of Figure 10 (upper right corner), dark lines perpendicular to the trench (horizontal in this figure), which are interpreted to be the faults shown in Figure 9, are prevalent, whereas in the south features parallel to trench, which are interpreted to be the outcropping beds in Figure 9, prevail. The abrupt and noticable change in the acoustic nature of the side-scan suggest that the northern and southern slopes are not responding equally to stress. Shallow structure differences may be the result of local stress regimes that act unequal due to nonuniform rates of fore-arc subsidence.

Southern upper-slope. The southern part of the upper-slope in Figure 10 (lower right corner) is relatively undisturbed, and appears to be a typical outcropping section of Lima Basin strata. The side-scan image of the southern upper-slope shows a banded pattern of

34

Plate II. SeaMARC II bathymetry of the upper-slope basin contoured at 100 m interval.

Fig. 10. a) SeaMARC II side-scan sonar mosaic of the upper-slope basin area. Light colors are low-intensity returns and represent unconsolidated sediment. Dark colors are high-intensity returns and represent outcropping strata and topographic relief. The light colored oval area is the upper-slope turbidite pond. White areas are gaps in coverage and uniform gray lines represent below ship's track. b) Trace diagram of the SeaMARC II side-scan naming main features. See also Figures 8 and 9.

PLATE II

78°50'W   78°40'W

11°20'S   11°10'S

Trench

11°30'S   11°20'S

78°30'W

Fig. 10 **A**

0   10KM

B

Hemipelagic
Sediment

Debris Blocks

Turbidite Pond   Debris Channels   Data Gap

Mid-slope   Northern Upper-slope

Normal Faults

Data Gap

Canyon   Outcropping Strata

Exposed
Strata

Structural High

Slump

Mid-slope   Slump
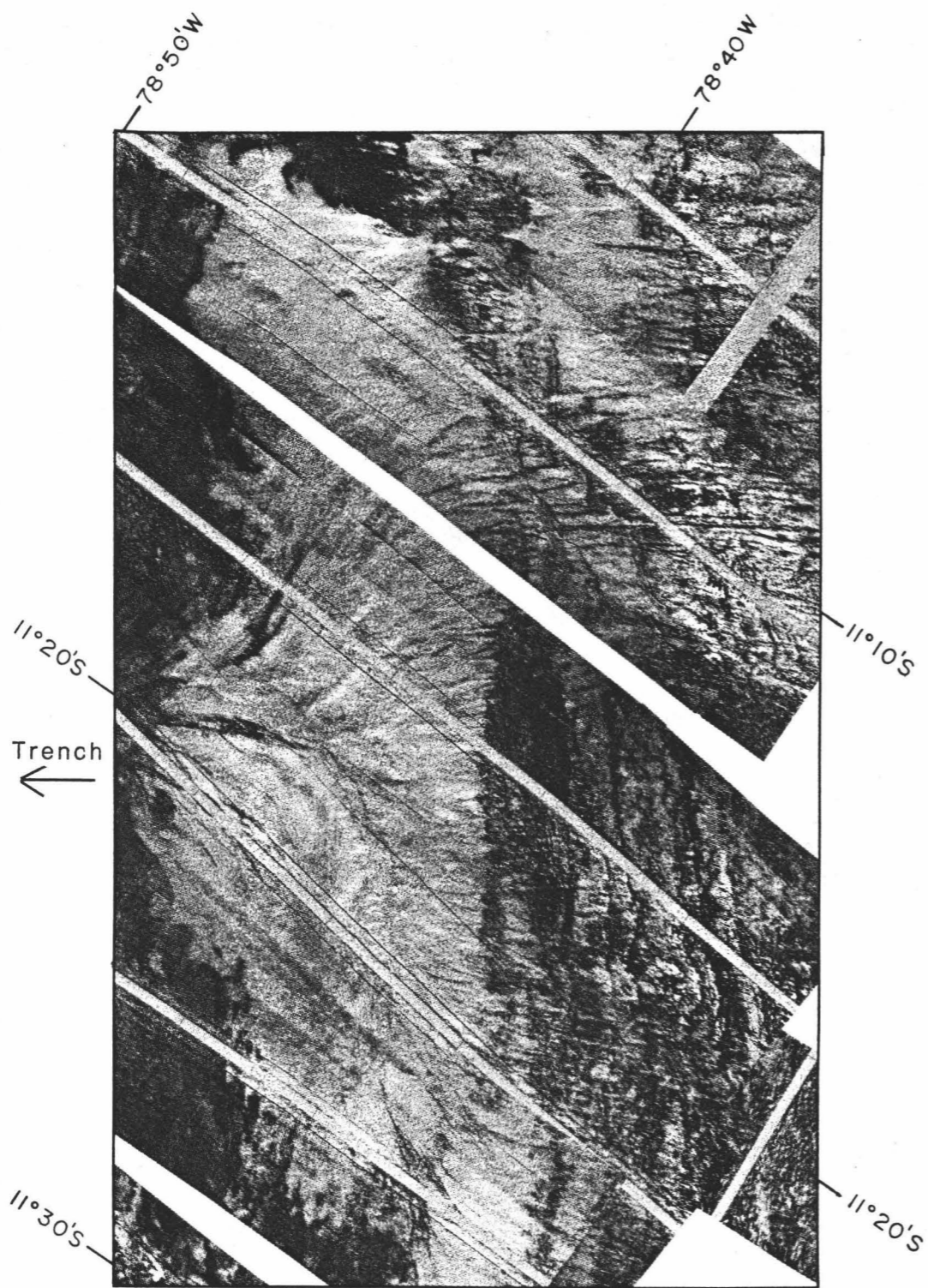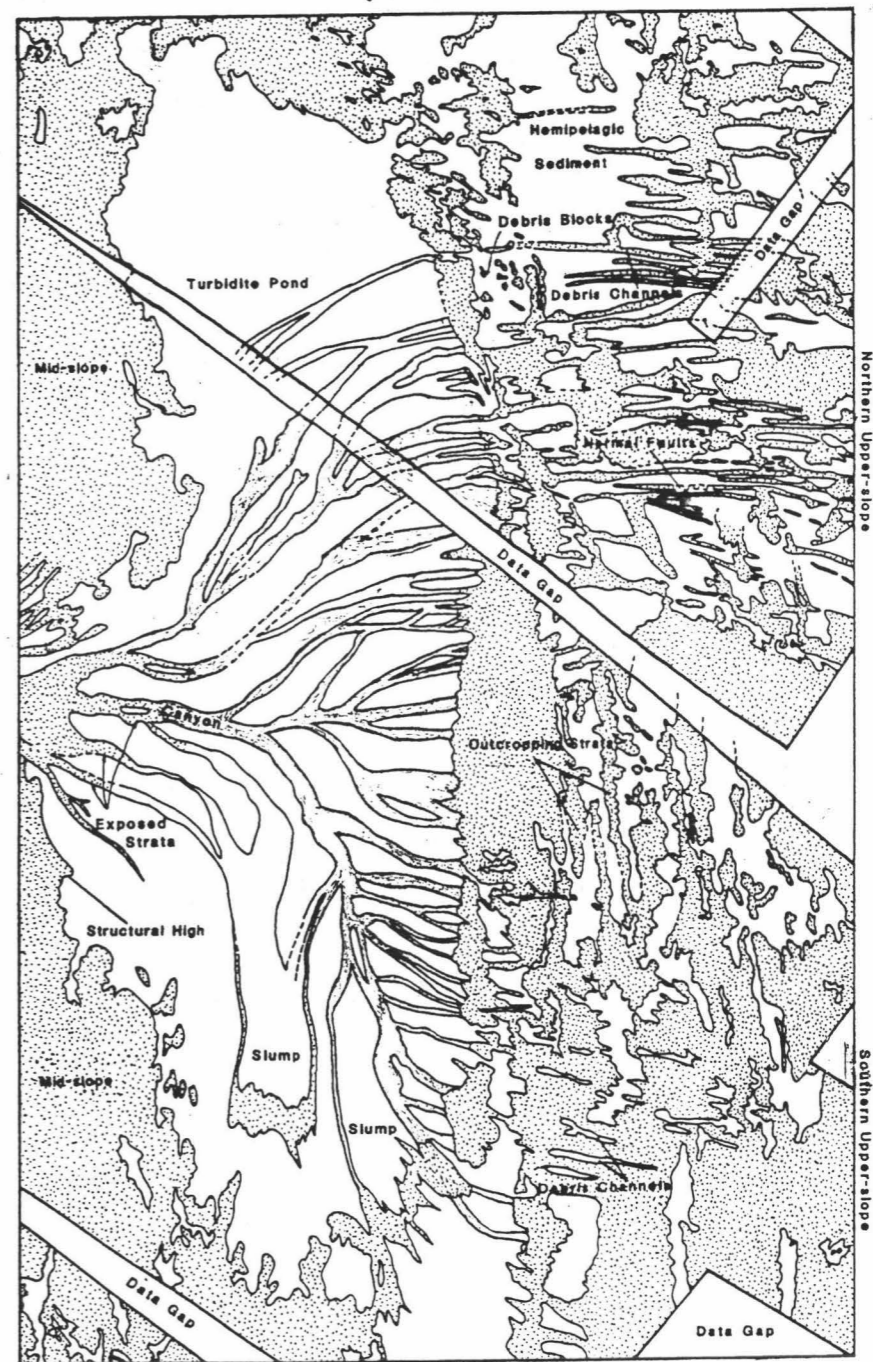
Debris Channels   Southern Upper-slope

Data Gap   Data Gap
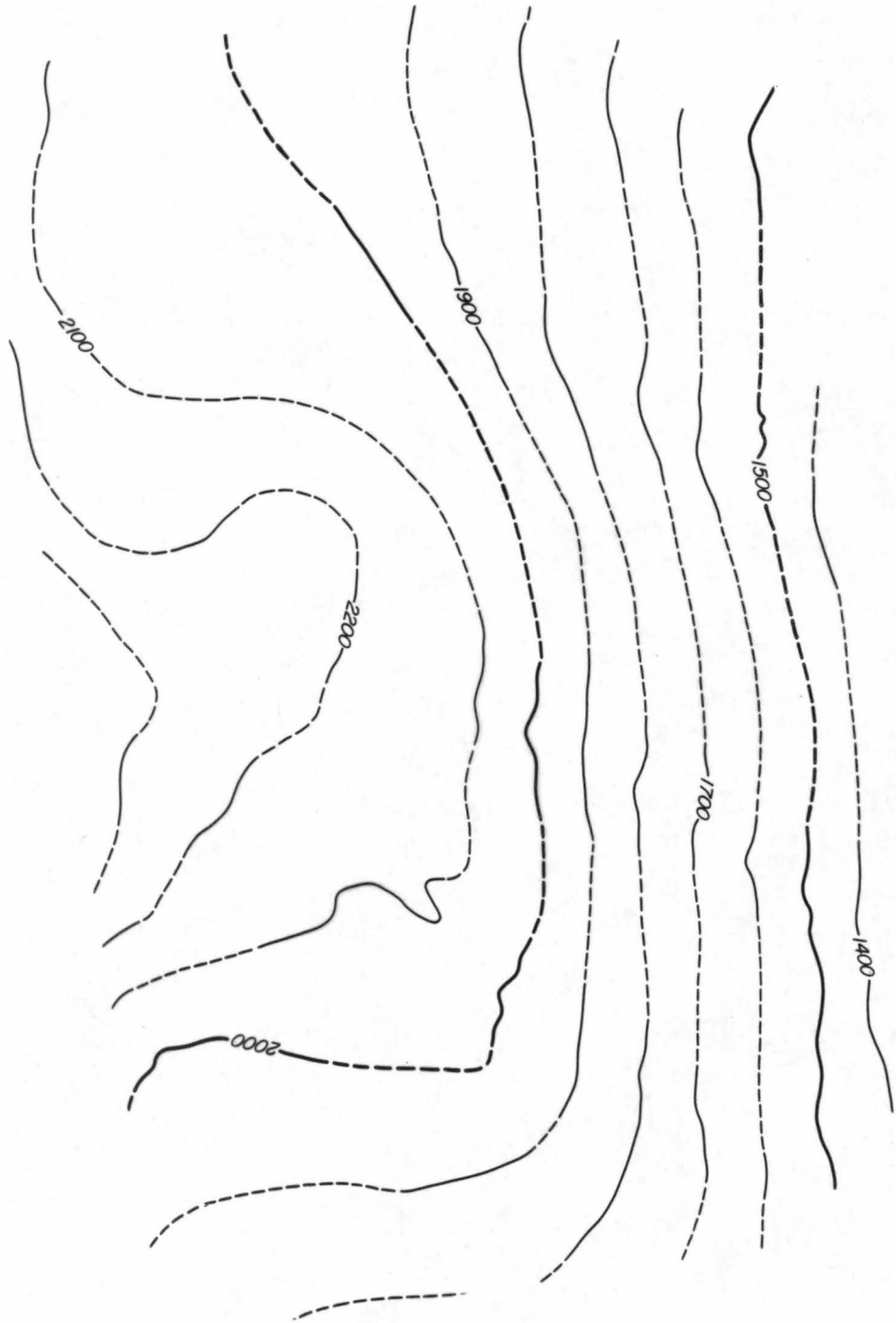
alternating dark and light returns (lower right corner, Figure 10a)

striking semi-parallel (N 40°W) to the trench. The dark bands probably

represent outcropping lithified sediments, while the lighter returns

corresponds to hemipelagic sediments (Figure 10a). Although the dark

bands could be mistaken for fault scarps, they appear equally dark on

both sides of the swath, indicating that the dark return is a

characteristic of the outcrop texture and not due to the topographic

relief of a fault scarp.

A single-channel seismic profile (Figure 11) shows outcropping

strata protruding along this slope. The outcropping beds form small

structural terraces that temporarily trap sediment. The resultant

steps of outcrops with intervening trapped sediment gives the southern

upper-slope its distinct appearance of alternating dark and light

banding on the side-scan. Even though the seafloor slope is only about

3° (Plate II), the overlaying hemipelagic mud has been eroded, exposing

the dolomite, mudstone, siltstone, etc., of the Lima Basin section.

The strata crop out with a dip nearly horizontal along the 2^O - 3°

slope, making the beds appear more extensive on the side-scan image

than their actual thickness would suggest. The more easily eroded

strata is differentially removed leaving beds of highly reflective,

more resistant material intercollated between beds of poorly reflective

less resistant sediment.

The more resistant layers are almost certainly dolomite. Chunks

of dolomite have been dredged; these are typically a few tens of

centimeters in size, and are believed to represent the total thickness

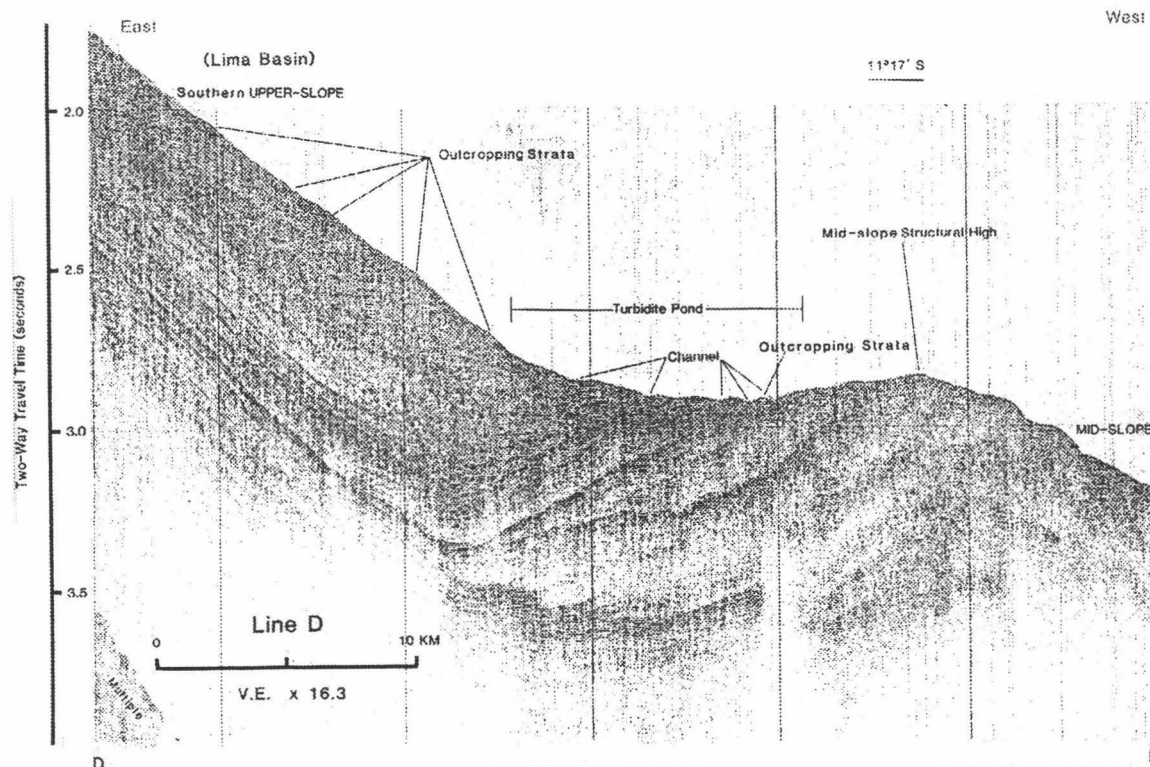Fig. 11. A single-channel seismic air-gun profile (Line D) across the southern upper-slope. See Figure 9 (D - D') for the exact location. Outcropping strata act as structural highs that trap sediment, preventing it from moving down slope. A more extensive mid-slope structural high retains sediment in a turbidite pond. Depositional channels on the turbidite pond are aligned in an out of the page.

of the dolomite beds [L. D. Kulm, personal communication, 1985]. The geologically similar Franciscan formation in California is believed to be a subaerial analogue of the Lima Basin section, and contains similiar dolomite beds on the order of centimeters thick. From consideration of the Franciscan, Kulm et al. [1984] concluded that the Lima Basin dolomite beds are of comparable thickness and distribution and therefore represent about 10 % of the total section.

That the dolomites represent only a fraction of the total section is supported by seismic data. Hussong and Wipperman [1981] measured a compressional wave seismic velocity of 2.2 km/sec in the uppermost Lima Basin section, whereas the velocity of dredged dolomite rocks has been measured at 5.6 km/sec [L. D. Kulm, Personal Communication, 1985]. Thus, although the individual dolomite layers have a high seismic velocity, the overall section is characterized by a much lower total velocity, which further support the conclusion that only a small portion of the upper Lima Basin section is dolomite.

The sedimentary rock outcrops on the southern upper-slope are fairly continuous and undisturbed along their strike and are only crossed sporadically by small intermittent channels (Figure 10a). These channels are light colored (thus low reflectivity) on the image, and, are perpendicular (N 50°E) to outcropping beds. Most of the unconsolidated sediment cover has been eroded and some has been redeposited down slope in the turbidite pond. The remainder of the fine-grained sediment cover, which is expressed as a light return on

the side-scan, is either trapped behind outcrops or within the thalweg of the cross-cutting channels (lower right corner of Figure 10a).

Northern upper-slope. The northern upper-slope is distinctly different from the southern upper-slope in that the northern upper-slope has a more gentle gradient of 2°, and has a more persistent hemipelagic sediment cover (Figure 10a upper right). However, even on this 2° slope the surface sediment is actively eroding and being redeposited in the turbidite pond below.

The preponderance of normal faulting trending perpendicular to the trench (N 60°E) in the northern upper-slope also distinguishes it from the relatively undisturbed southern area. On the SeaMARC II side-scan image the fault scarps are parallel dark lines perpendicular to the strike of the trench-axis (Figure 10a). A single-channel seismic reflection record (Figure 12) shows an oblique crossing of these normal faults. Most of these normal faults appear to be down-thrown on the northwest side. The faults scarps are not recognized on the bathymetry contoured at 100 m (Plate II). The normal faulting in this part of the upper-slope may be caused by tectonic readjustment.

Debris flow channels form along the fault traces, which serve as the channels for the removal of sediment from the upper-slope. These channels appear dark on the side-scan image (Figure 10a) due to the rough surface texture of the fault breccia and or the large size of the debris in channel. Although most of the normal faults are downthrown in the same direction, some have formed grabens from which sediment has not eroded, obscuring the outcropping beds observed elsewhere.

Fig. 12. A single-channel seismic air-gun profile (Line E) across the northern upper-slope. See Figure 9 (E - E') for the exact location. This is an oblique crossing of the normal faults on the upper-slope trending perpendicular to the trench-axis. Many exist however only three are labeled. The oblique crossing and the small throw on these faults makes them difficult to identify in this low frequency reflection record. The faults are far more obvious in the surface morphology (Figure 10).

Normal faulting is also found parallel to the trench in the upper-slope basin, based on interpretation of reflection seismic multichannel records [von Huene, 1985; Hussong and Taylor, 1985]. The side-scan mosaic coverage does not show conclusive surface expression of these trench-parallel normal faults.

Upper-slope turbidite pond. Sediment eroded from the southern and northern upper-slope is deposited in a pond of turbidite sediments (Figure 10a). Oval-shaped in appearance, this sediment pond has an aerial extent of about 400 km^2 and lies in water depths of 2000 m to 2200 m (Plate II). The sediment of the turbidite pond has a maximum thickness of approximately 40 m.

In the southern part of the large turbidite pond slumping occurs with a slippage surface between the base of the hemipelagic section and the older sedimentary rocks of the upper-slope. It appears that large sheets of the hemipelagic section are coherently sliding downhill, uncovering the Neogene strata underneath. Additional sediment transport has formed marginal shear channels along the sides of the slump (Figure 10b). These marginal shear channels form the primary channels with secondary channels entering at near perpendicular angles from the upper-slope. Sediment eroding from the southern upper-slope flows directly into the primary channel in the turbidite pond and then into a main canyon (Figure 13 and Figure 10a left middle margin). The channel on the west of the slump is thus apparently starved of upper-slope sediment, resulting in a more faint image on the side-scan (Figure 13). Presumably the acoustic fading is low amplitude echoes
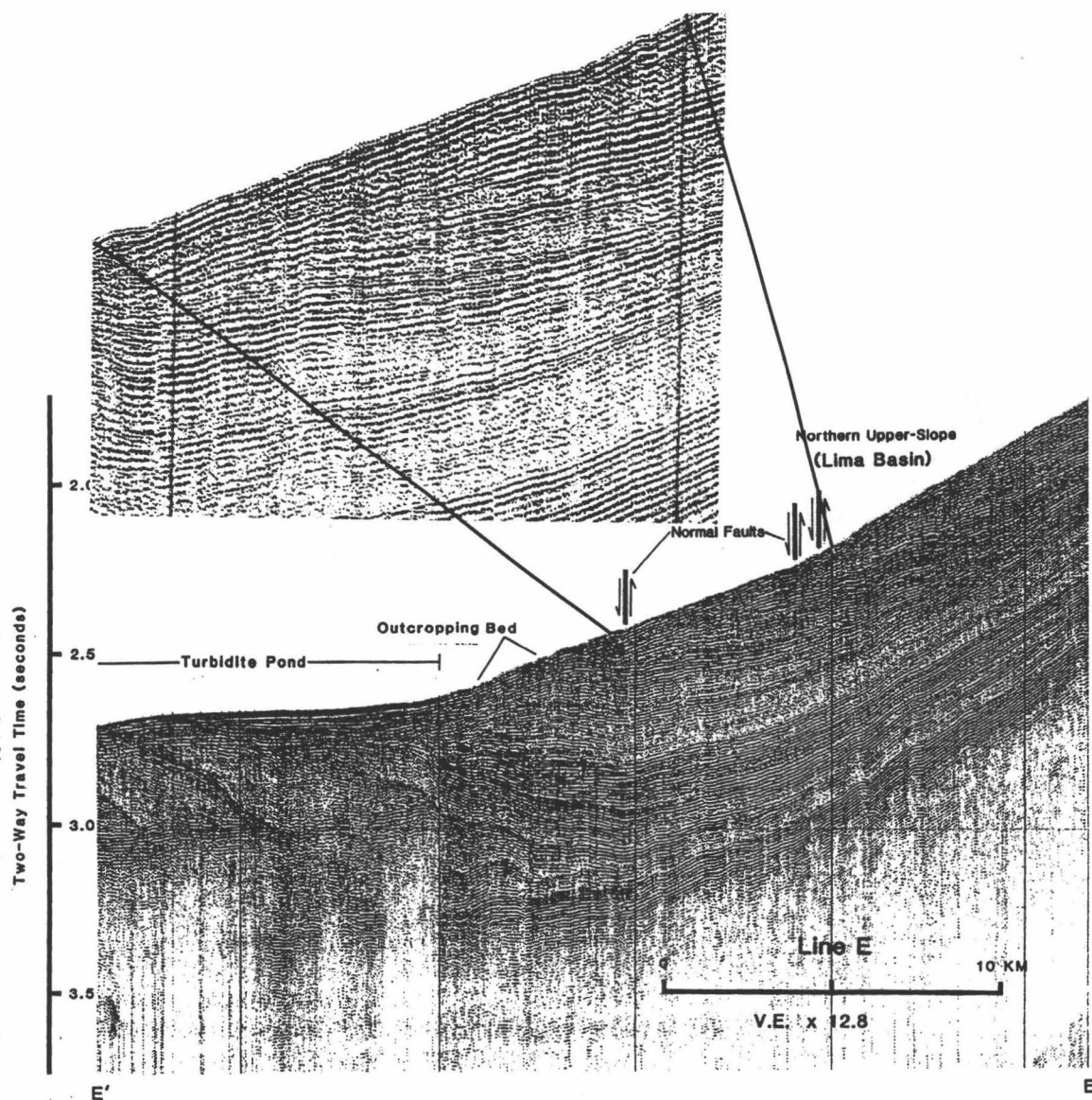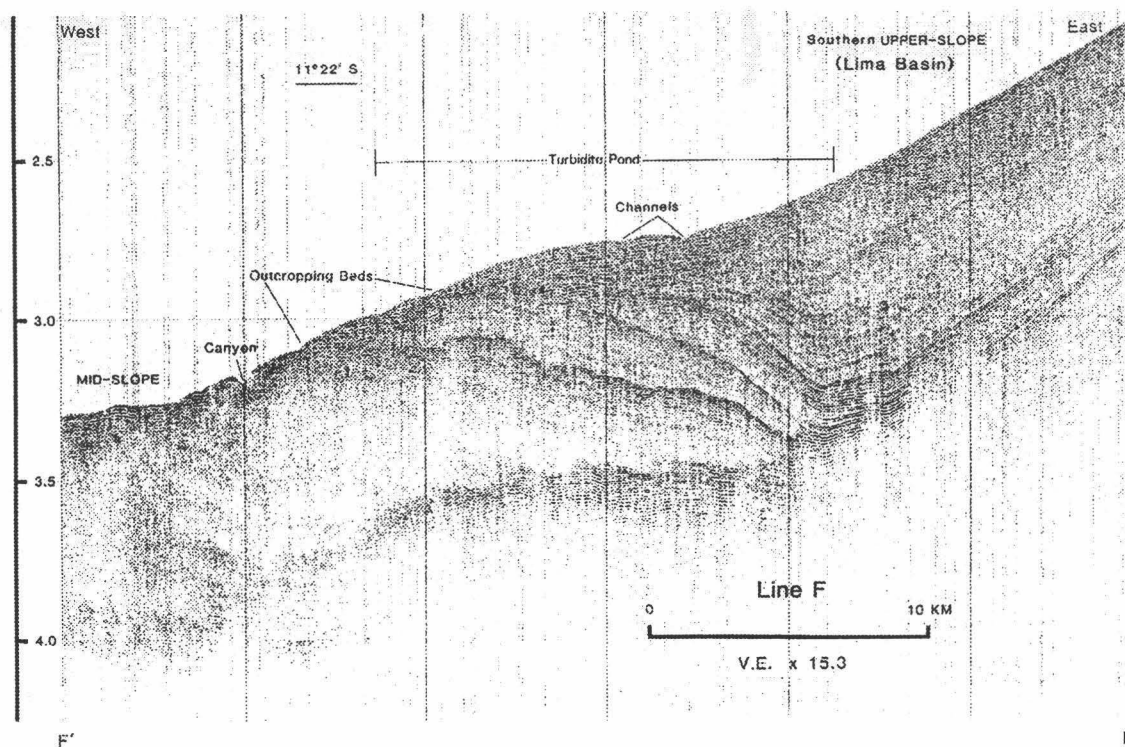
Fig. 13. A single-channel seismic air-gun profile (Line F) across the southern upper-slope. See Figure 9 (F - F') for the exact location. Two main channels that run north and south (in and out of the page), eventually connect with a main canyon that dissects the mid-slope. The channel on the right has pirated the adjacent channel on the left.

from muds that have settled in the channel, partially obscuring the rough texture of a more active channel (Figure 10a).

Many of the northern upper-slope faults extend to the edge of the turbidite pond and continue on as channels (Figure 9 and 10b, upper right corner). The channels in the turbidite pond and the adjacent upper-slope regions form an intricate network which is analogous to a "drainage network" in the subaerial environment.

Upper-slope submarine "drainage network": Using Howard's [1967] compilation of drainage patterns, the Lima Basin can be described using analogous terrestrial morphologic names. The drainage network is complex; trellis pattern on the upper-slope and pinnate pattern in the turbidite pond, but individual channels may be braided or meandering (Figure 10b). These channels all coalesce into a narrow, deeply incised canyon which bisects the mid-slope in the ensonified area. Figure 13 shows the turbidite pond and canyon near where it breaches the structural high of the mid-slope.

The location of the breach in the mid-slope is controlled by a structural low in the basement. The upper-slope and mid-slope may be fractured by a fault trending N 60°E, perpendicular to the trench axis. This may be the same large fault that bounds the change in slope between the northern upper-slope and the southern upper-slope.

SeaMARC II acoustic images have often been compared with aerial photographs and side-looking radar imagery, especially for features such as volcanoes and seamounts. The familiarity with optical images helps make acoustic images more understandable. Although the processes

are different between the subaerial and submarine environments, the comparisons offer an insight on difficult concepts.

A similiar comparison can be made between the Lima Basin image of a submarine drainage pattern and a subaerial drainage pattern in the State of Nebraska (Figure 14). In Nebraska, the smaller secondary rivers flow down into a primary river (Platte) which in turn bends to enter the regional base level of the main river (Missouri) (Figure 14). The regional gradient of Nebraska is gentle, and the parallel channels have been eroded by water and wind and have dissected an older plain. Layers of older sandstone, shales, and limestones are near-horizontal, and are overlain by easily eroded wind-blown unconsolidated sediment (loess).

Thus, although the Lima Basin drainage network is only 7 % the size of Nebraska's system, there are gross similarities in the relative proportions of the "drainage networks". The comparison lies in the similarity of slopes and unconsolidated sediment overlaying a section of consolidated bedrock. Both the areas are eroding because the base level has been lowered, prompting the removal of easily eroded material.

Mid-slope

The mid-slope is the transitional area between the mid-slope basin and the upper-slope basin and is between 2200 m and 3750 m depth
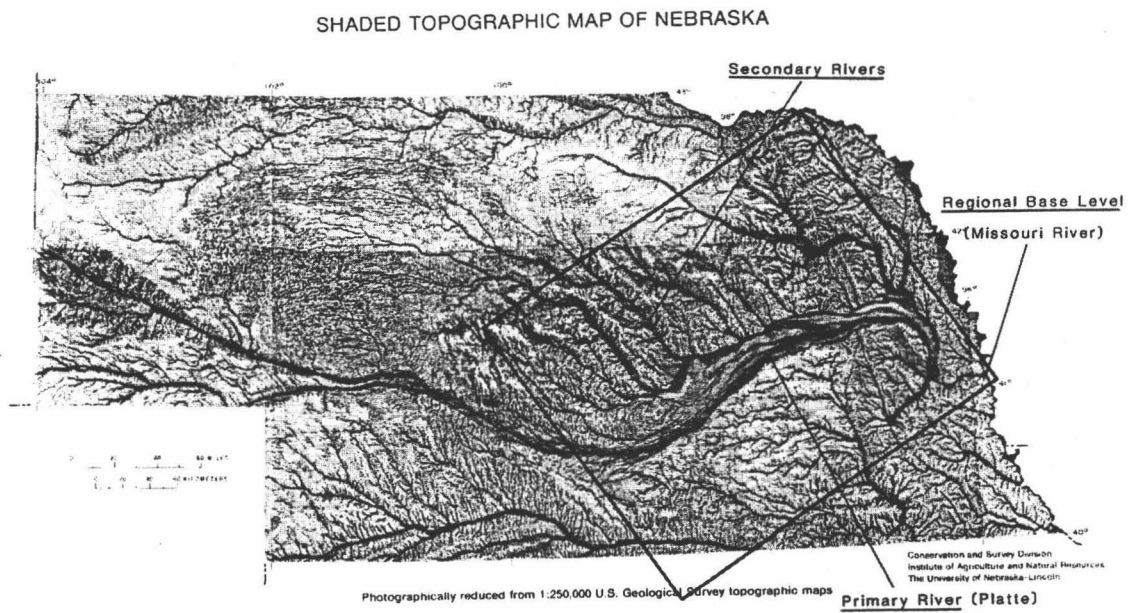
SHADED TOPOGRAPHIC MAP OF NEBRASKA

Fig. 14. Shaded relief map of the State of Nebraska. The box shows the eastern drainage system of this state. This area has been compared to the submarine "drainage system" shown in the Lima Basin SeaMARC II mosaic (Figure 10b).

(Figure 15). The mid-slope seafloor has a regional slope of 3° to 5°. Erosion of the overlying hemipelagic sediment from this slope has exposed the deeper, older rocks of the lower Lima Basin section which are stratigraphically below the outcrops on the upper-slope.

This mid-slope has been dredged several times, yielding heavily tectonized dolomites and mudstones [Kulm et al., 1981b, Kulm et al., 1985]. Some of the dredged rocks have been fractured and re-cemented up to three different times, indicating a very disrupted regional tectonic history [Kulm et al., 1985].

To simplify the description of the mid-slope, it can be divided into three different areas: the northern, central, and southern mid-slope (Figure 15).

Northern mid-slope. The northern mid-slope (Figure 16) is a distinct sub-area that contains several features which may be related to the subsidence of the Peru fore-arc. A prominent feature is an outcrop located in the upper right corner of Figure 16. The similiar side-scan return from opposite look-directions indicates consistent texture across the outcrop, which in turn suggests a homogeneous unit. A dredge haul from this outcrop, (MW8506-11), indicated that the outcrop was composed mainly of dolomicrite (84%), brecciated dolomite (15%), and phosphorite (1%). The dip of the formation is very close to the slope of the seafloor and thus making the outcrop appear much more extensive. A normal fault, that trends perpendicular to outcropping strata (N 50^OE), forms the northern boundary (Figure 16b).
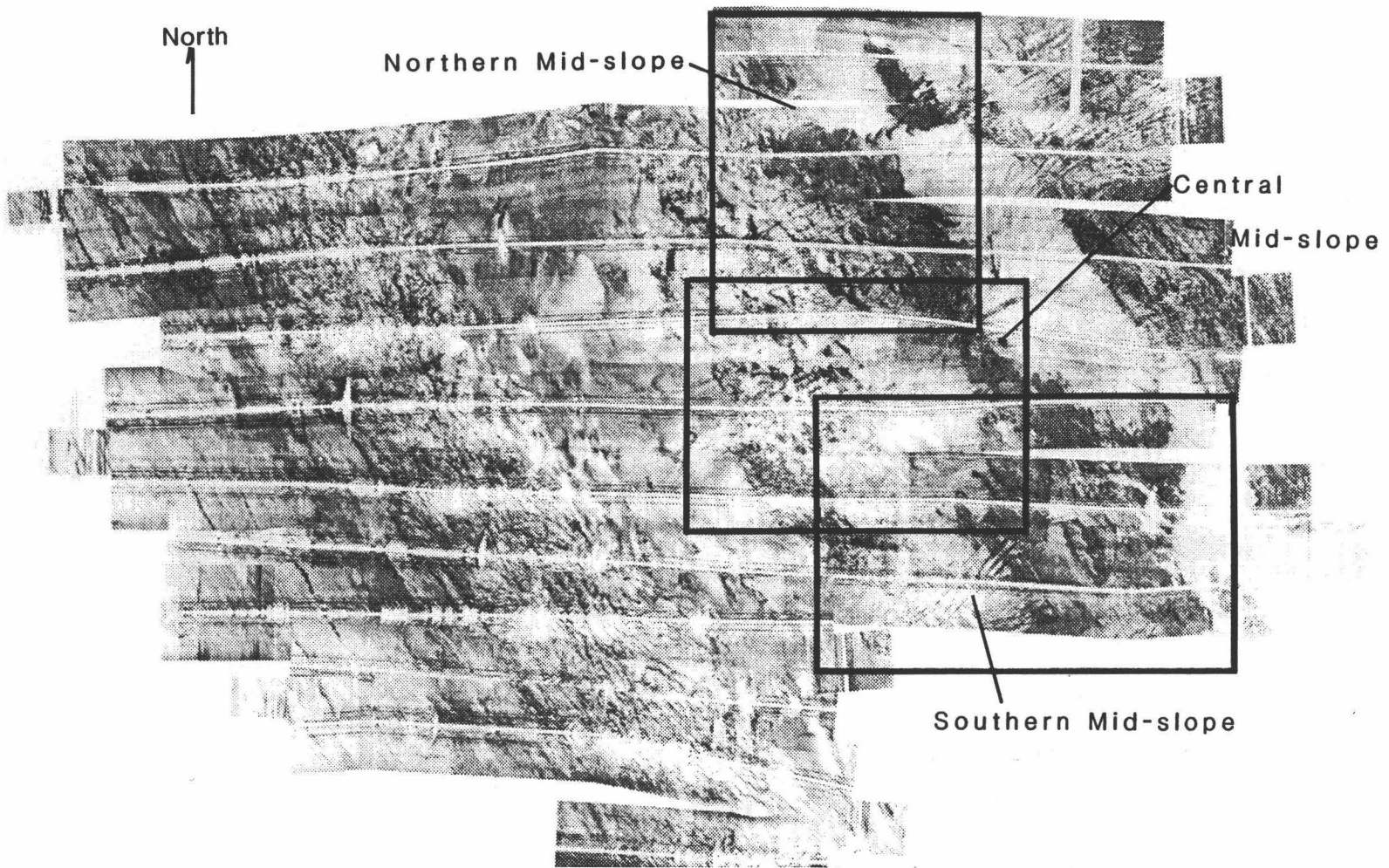
Fig. 15.   The mid-slope has been divided into three additional sub-

sections: northern mid-slope, central mid-slope, and southern mid-slope.

These outlined areas comprise Figures 17, 20, and 23 respectively.

49

Plate III.   SeaMARC II bathymetry of the northern mid-slope contoured at a 100 m interval.

Fig. 16.   a) SeaMARC II side-scan sonar mosaic of the northern mid-slope showing the outcropping strata and "kite-shaped" knick points. Light areas are sediment.   Dark areas are caused by relief and outcropping strata of the lower Lima Basin section.   b) Interpretive diagram of the northern mid-slope based on the general features of the side-scan.

PLATE III
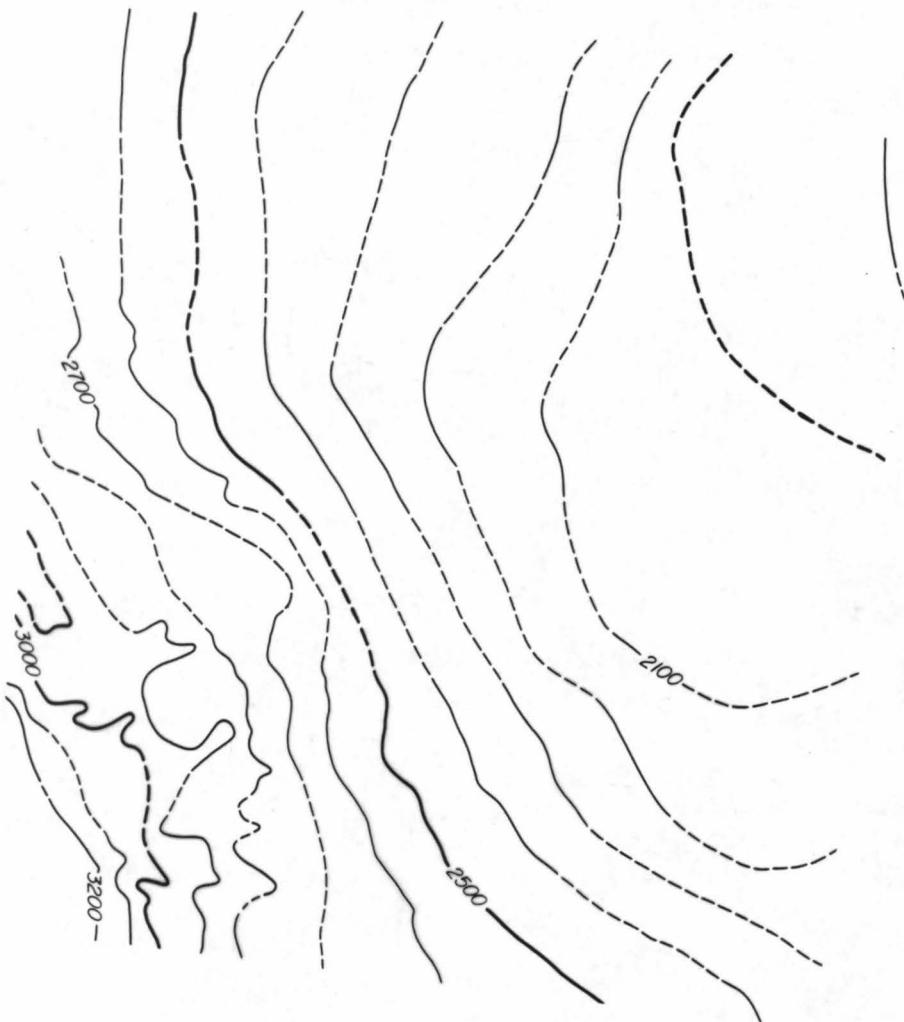
Fig. 16 A

B

Directly to the west of this outcrop lies a sediment-filled graben (Figure 16b). The southern normal fault which bounds this graben may extend under the sediment to continue as the 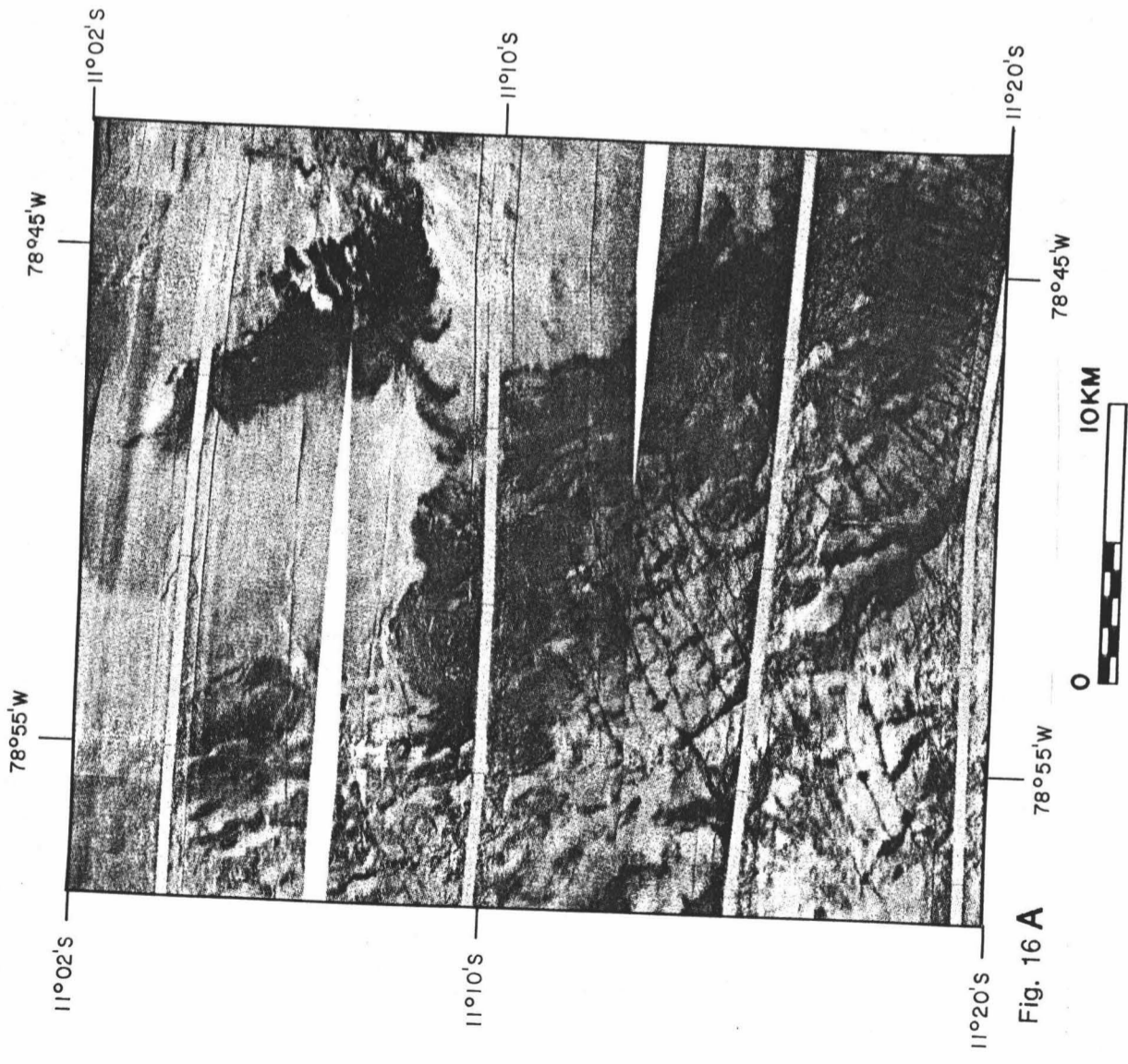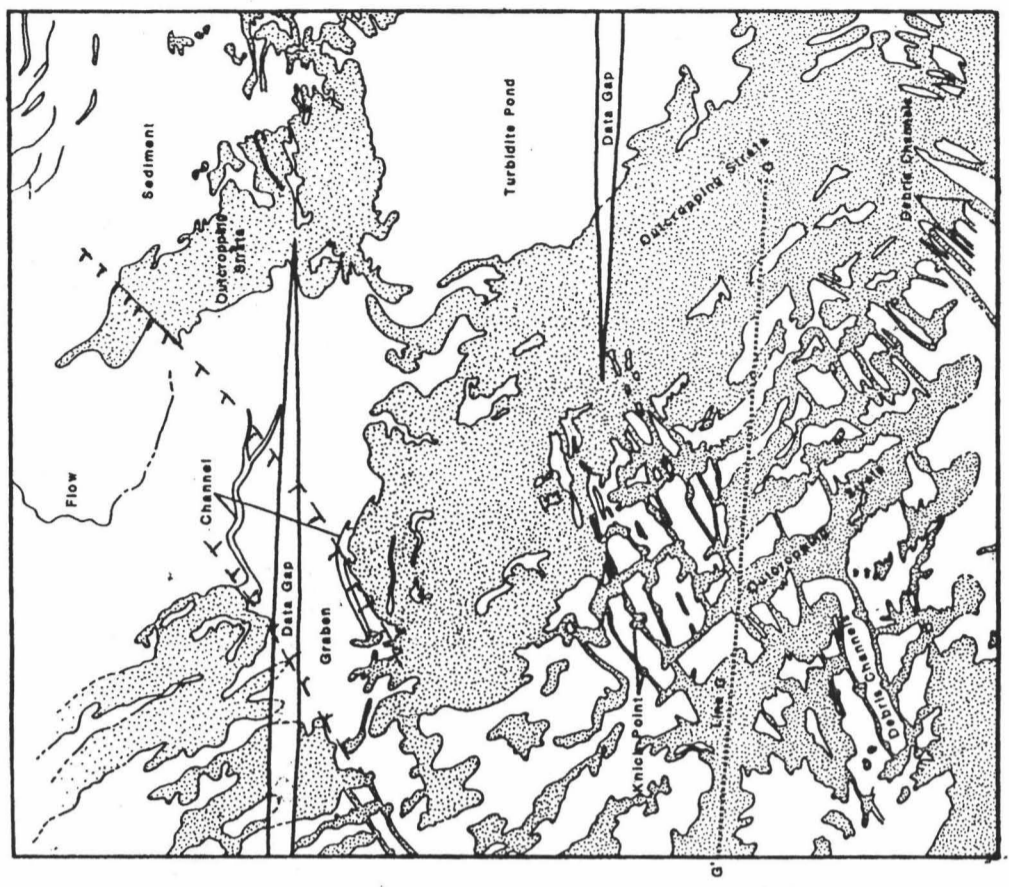same normal fault which helps expose the outcrop to the east (as drawn on Figure 16b). North of this graben there is an associated horst which has sufficient relief to avoid being covered by sediment. The graben serves as a path for the regional transport of sediment down-slope. Sediment channels appear on the normal faults bounding edges of the graben (Figure 16b). As the sediment moves down the 3° to 4° slope it temporarily collects on small step-like terraces. Figure 17 is a single-channel seismic profile across the northern mid-slope that crosses these 1 - 3 km wide terraces.

Also distinctive on this mid-slope area are the kite-shaped features that interrupt the dark linear debris flow channels (Figure 16a, lower left corner). Since the debris channels trend perpendicular to outcropping strata, the kite-shapes are apparently knick-points where erosion has caused gullies to be incised into the outcrop terraces (Figure 18).

Central mid-slope. The second distinct sub-area of the mid-slope area (2200 m to 3800 m water depth) is the central mid-slope (Figure 19). This area is largely sediment covered and is characterized on the side-scan by a distinctive triangular area of generally low backscatter toward the base of the slope (Figure 19a). Some of the eroded sediment from the upper-slope has moved down-slope through the channels and has been deposited temporarily at the mouth of the main canyon (at the
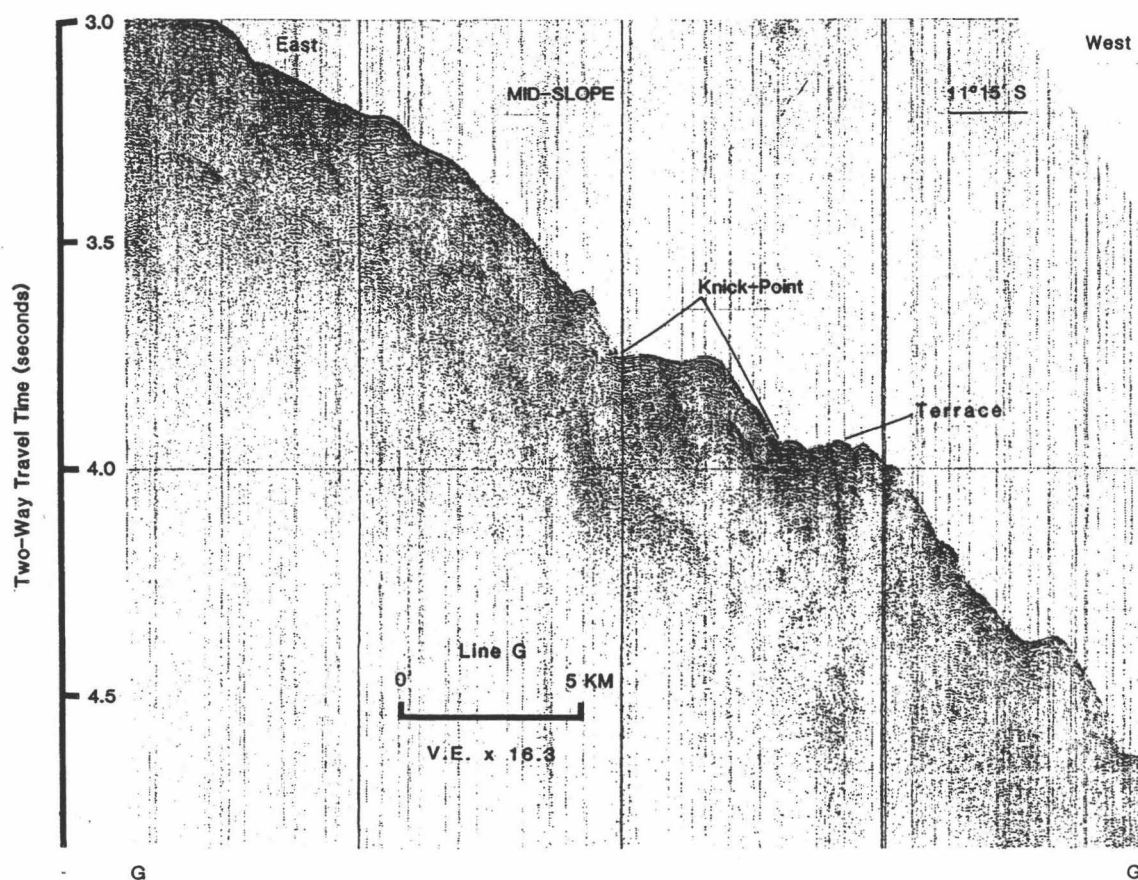
Fig. 17. A single-channel air-gun seismic profile (Line G) across
the northern mid-slope area. See Figure 17b (G - G') for the exact
orientation. Debris-channels that transect the slope are affected by
step-like terraces causing gullying which creates kite-shaped (knick-
points) dark images on the side-scan (Figure 17).
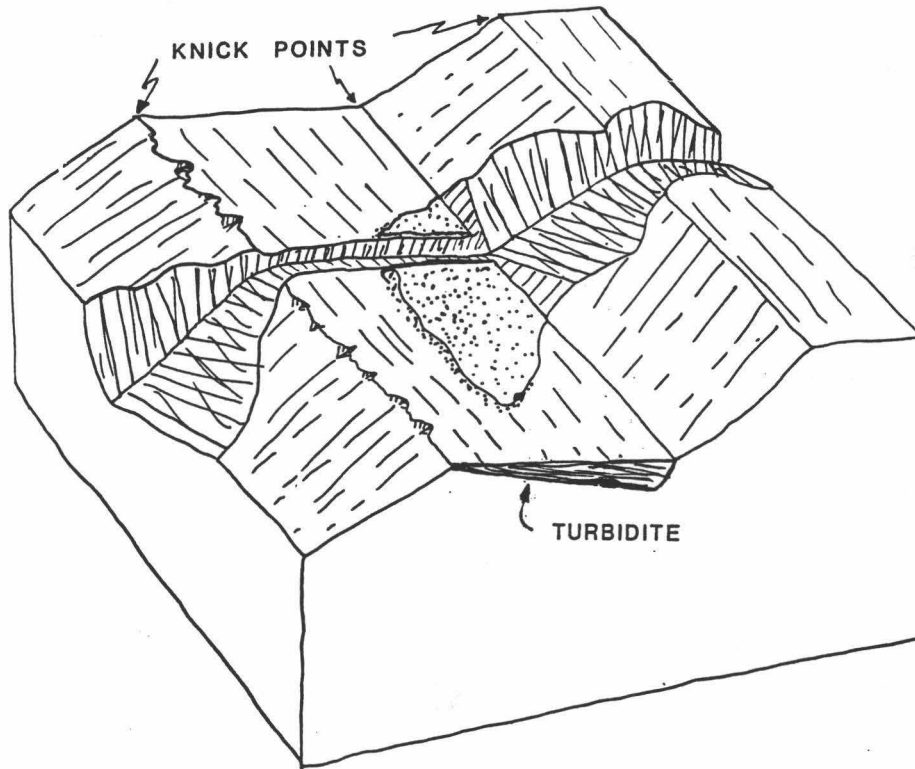
Fig. 18. Dark kite-shaped side-scan returns in the northern mid-slope area are explained by this interpretive block diagram. Debris channels encounter knick-points (inflection points) on a terraced slope caused by normal faulting and outcropping strata.

55

Plate IV.   SeaMARC II bathymetry of the central mid-slope contoured
at a 100 m interval.

Fig. 19.   a) SeaMARC II side-scan sonar mosaic of the central mid-
slope area. b) Interpretive diagram of the central mid-slope based on
the features seen in the side-scan. The trapezoid in the middle of the
diagram outlines an area believed to be disturbed by slides and
slumping.   This area also may contain mud-volcanoes.

PLATE IV

79°00'W   78°50'W   78°40'W

11°20'S   11°20'S

11°30'S   11°30'S

79°00'W   78°50'W   78°40'W

Fig. 19 **A**

0   IOKM

Debris Channel

Main Canyon

Outcropping Strata

Sediment

Mud-volcanoes

H'   Line H   H

Slumping Sediment

Debris Channel   Data Gap

MID-SLOPE BASIN
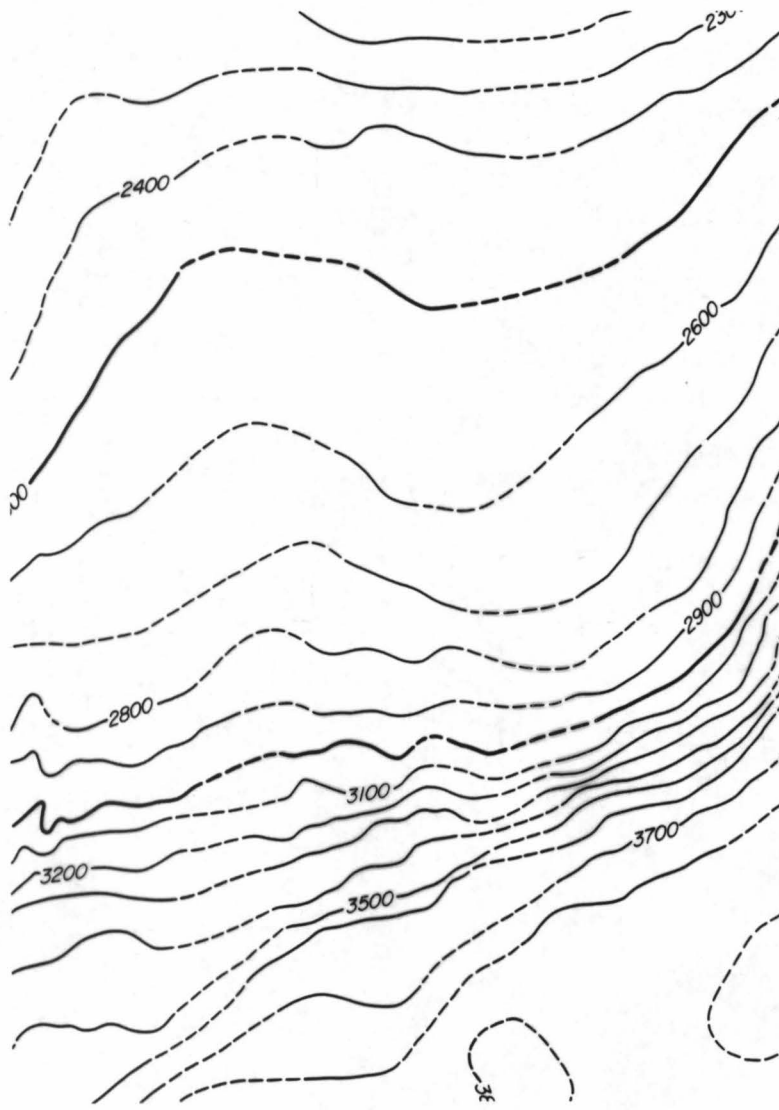
Outcropping Strata

B

northeast corner of Figure 19b). The sediment in this area has temporarily collected on a 4° to 5° slope and has a fan-shaped appearance, but lacks the classical form of a shallow water deltaic fan. The fan-shaped accumulation of hemipelagic sediment is about 45 m thick, although the poor quality of the single-channel seismic records makes this thickness uncertain (Figure 20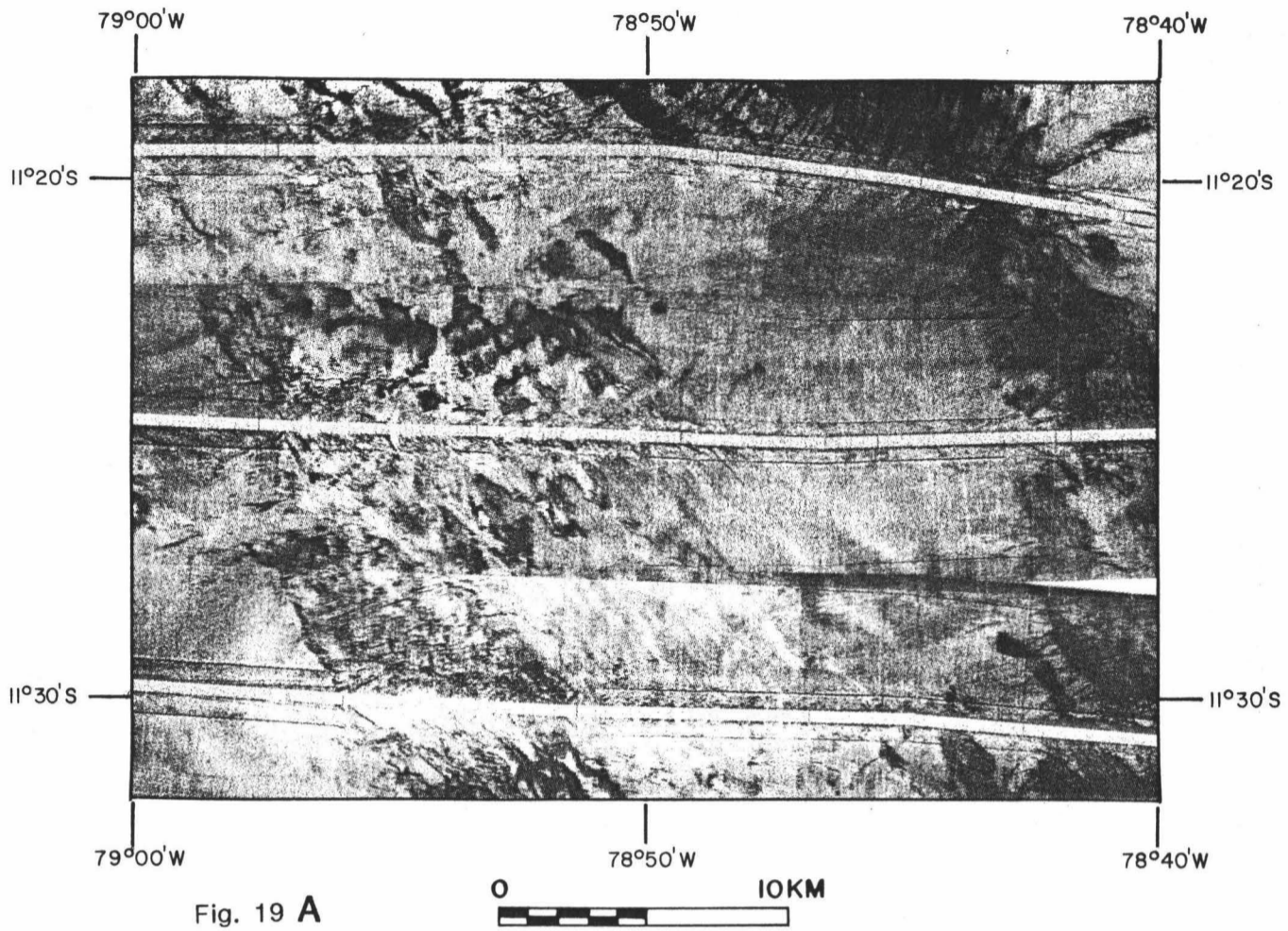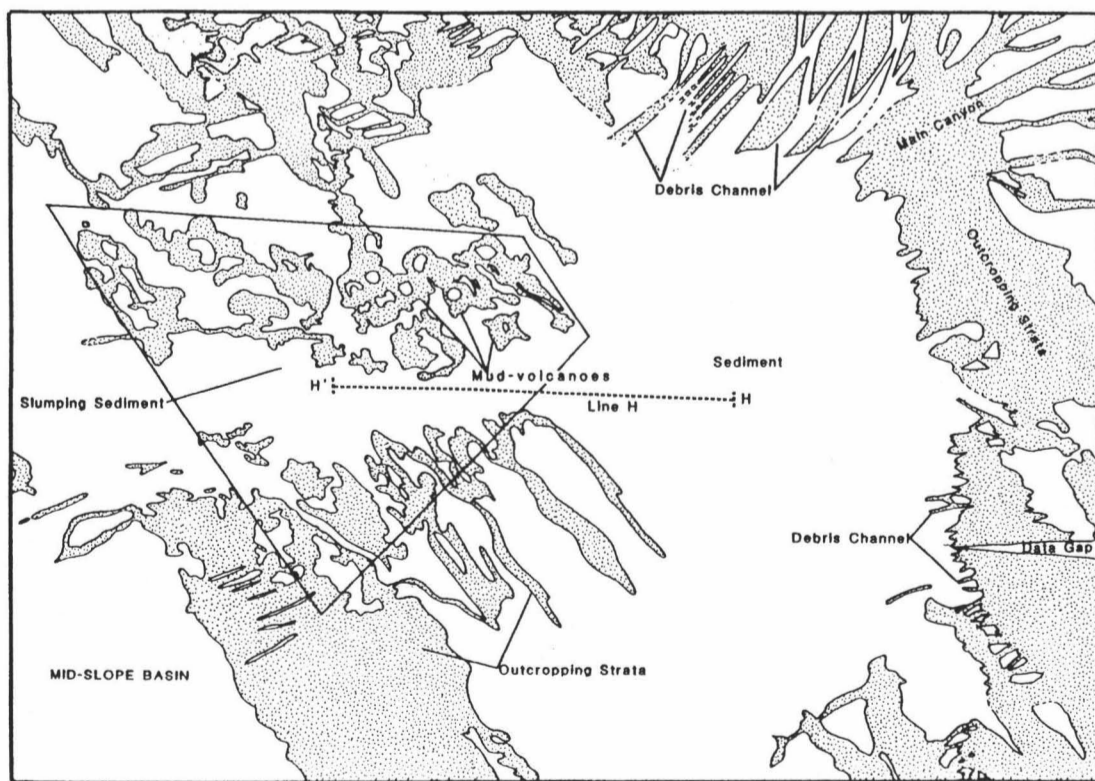). The shape of the sediment accumulation, and its location, may be controlled by the basement morphology of the Upper Slope Ridge which bifurcates in this area (Figure 3).

Debris flow channels appear as dark lines on the side-scan across the barren outcropping strata of the lower Lima Basin section on both sides of the mouth of the main canyon (upper right corner of Figure 19a). These channels appear to have very rough sides with little or no fine-grained hemipelagic sediment deposited in them. The debris channels are quite straight and have few tributaries (Figure 19b). The slope of the seafloor in this area is relatively steep, about 5° (Plate IV). These debris channels look like, and may behave in similar fashion to, avalanche shoots on the land. Material that flows down these channels comes from the eroded Lima Basin section, including the brecciated dolomites and other coarse sediment components. Apparently the channels have little fine-grain sediment input, except for the main canyon, due to the mid-slope structural high that blocks fine-grained material from entering from the upper-slope turbidite pond.
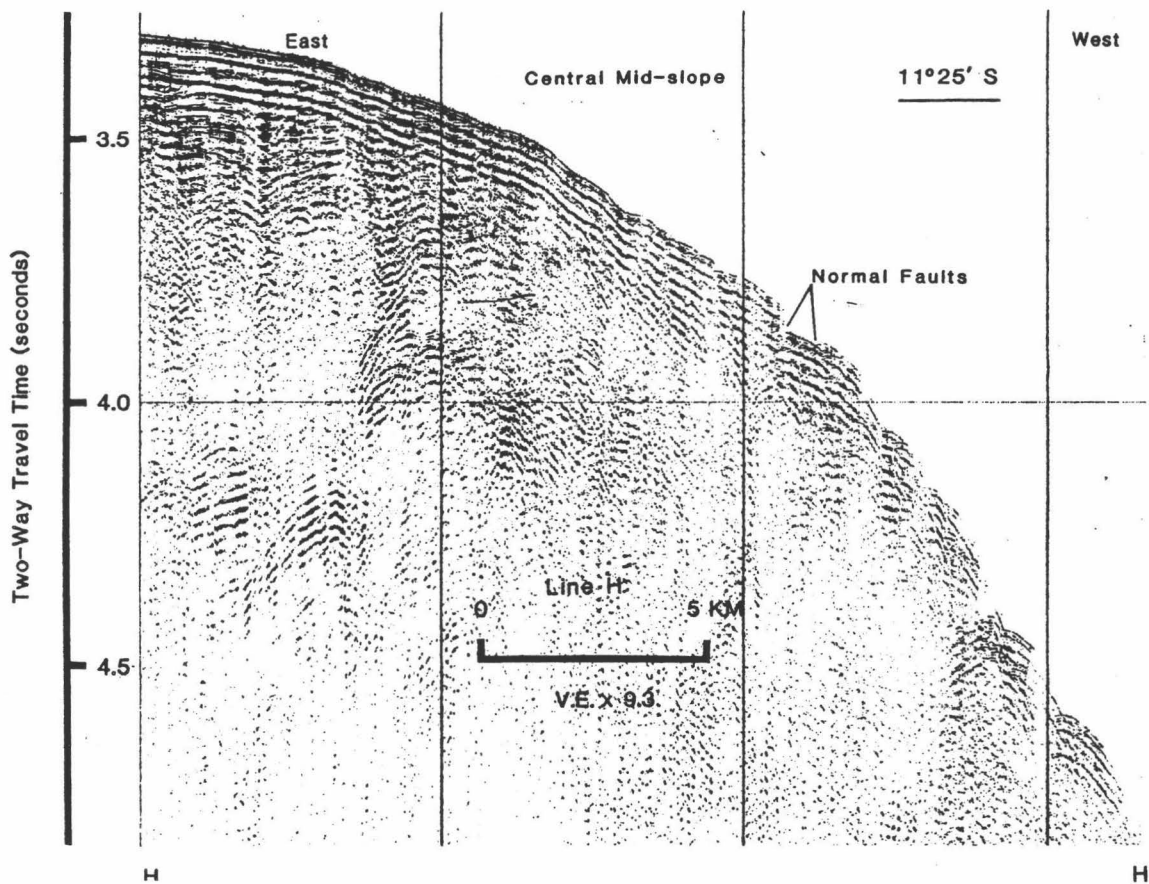
Fig. 20. A single-channel air-gun seismic profile (Line H) across the central mid-slope. See Figure 20b (H - H') for the location. Normal faults occur parallel to the trench-axis which may help create pathways for fluid to escape and create mud-volcanoes.

At water depths of 2800 m to 3200 m, possible mud-volcanos are observed on the side-scan and (even more tentatively) from single-channel seismic and 3.5 kHz sub-bottom profiles. The side-scan mosaic shows a circular feature of uniform dark reflectivity relative to surrounding sediment. Mud-volcanoes are known to occur both on land and off shore; when underwater they have typical base diameters of 2 km and heights of 60 m [Hussong, 1985]. They have also been described as seabed depressions caused by the evacuation of material from below [Westbrook and Smith, 1983].

In the Peru fore-arc region the source of the fluids emitted from the mud volcanoes has been suggested as occurring in the fore-arc basin deposits, fractured metamorphosed crust, or the subducting oceanic slab. If the fluids are derived from the subducting slab, the location of the mud volcanoes may suggest that they are penetrating through the fore-arc along the contact between the accretionary prism and the metamorphic block composing the ancient continental massif [Kulm, 1986]. In fact, the location of the mud-volcanoes in the lower portion of the central mid-slope, at the base of the slope leading into the mid-slope basin, is in agreement with the assumed location of the contact between oceanic crust and continental crust beneath the overlying accretionary prism. If, as has been suggested, this area is faulted perpendicular to the trench-axis, the alignment of the mud volcanoes perpendicular to the trench would also be explained. In deed, a large fracture trending N 60°E that goes through the canyon and also sub-divides the upper-slope was proposed creating the mechanism for the release of fluid [Westbrook and Smith; 1983, Hussong, 1985].

SeaMARC II bathymetry (Plate IV) shows a shallow 5 to 6 km wide trough through the middle of this area where the mud-volcanoes appear. This could imply that the sediment in this heavily deposited area has exceeded parameters for failure and started to slump, along a surface between the older consolidated sediment surface and the base of the unconsolidated hemipelagic sediment. The overlying hemipelagic sediments on such a slump would be widely disrupted and could be the cause of the distinctive appearance of this portion of the side-scan image.

Southern mid-slope. The southern mid-slope is characterized by large debris flow channels on eroded slopes (Figures 21). The SeaMARC II bathymetry displays slopes with a gradient of 4° to 4.5°. The upper-slope hemipelagic sediments on the eastern side of Figure 21a seem not to be affected by slumping, and contain no channels such as occur in the adjacent turbidite pond to the north. The hemipelagic sediment is confined behind a structural high and prevented from moving down slope by the up-turned outcropping strata (Figure 11). As the accumulation of sediment exceeds the height of the confining structure it breaches the mid-slope high and cascades down, forming an over-flow channel (Figure 21b). The channels are sediment filled and appear light-colored on the side-scan image. The channels curve and may be controlled by normal faults at the head of a large slide feature below that is working its way up the slope.

This large slide feature comprises a major portion of the southern mid-slope sub-section (Figure 21b, dashed oval). It has a total extent

62

Plate V. SeaMARC II bathymetry of the southern mid-slope area,
contoured at a 100 m interval.

Fig. 21. a) The southern mid-slope area ensonified by SeaMARC II
side-scan. The white areas are gaps in the side-scan coverage. b)
Interpretive diagram of the southern mid-slope displaying features
identified from the side-scan. Dashed oval outlines a large slide
feature bordered by marginal shear channels.

PLATE V

78°50'W   78°40'W   78°30'W

11°30'S   11°30'S

11°40'S   11°40'S

78°50'W   78°40'W   78°30'W

Fig. 21 **A**

0   10KM

Sediment Cover

Outcropping Strata

Terrace

Data Gap

Terrace

Turbidite Pond

Slump Scar?

Marginal Shear Channel

Slump Block

Over-Flow Channel

Light Sediment Cover

Data Gap

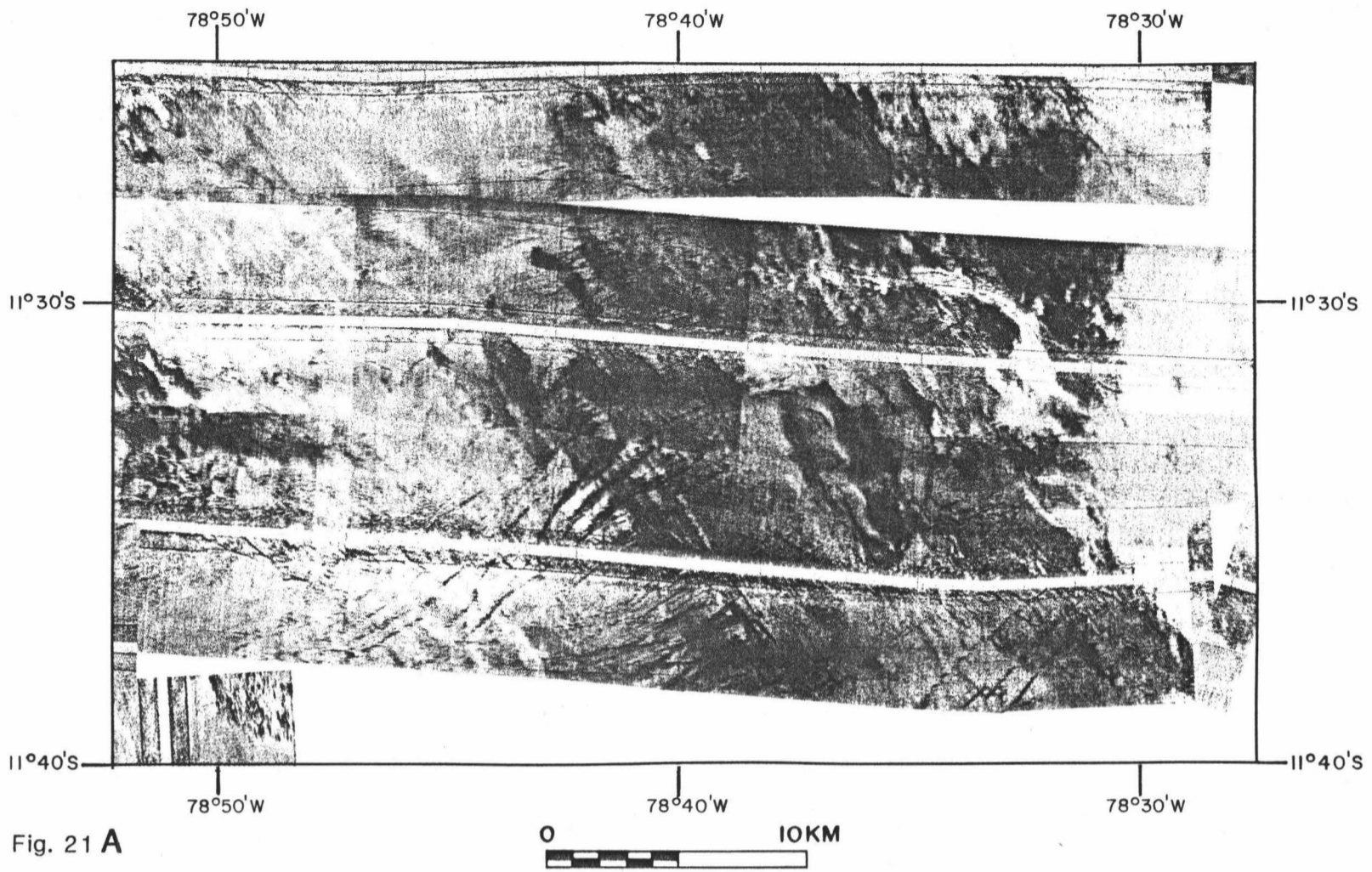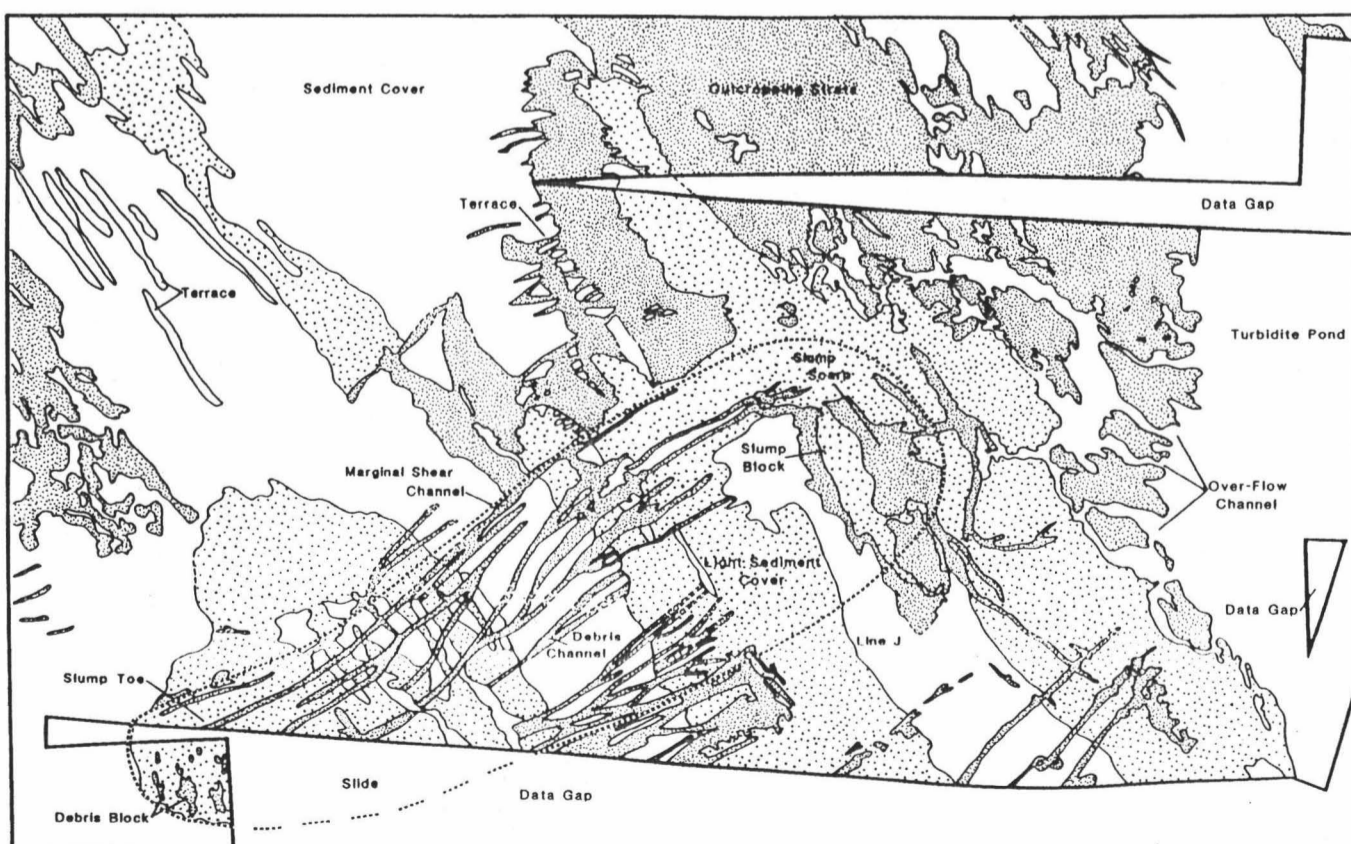Debris Channel

Line J

Slump Toe

Slide

Data Gap
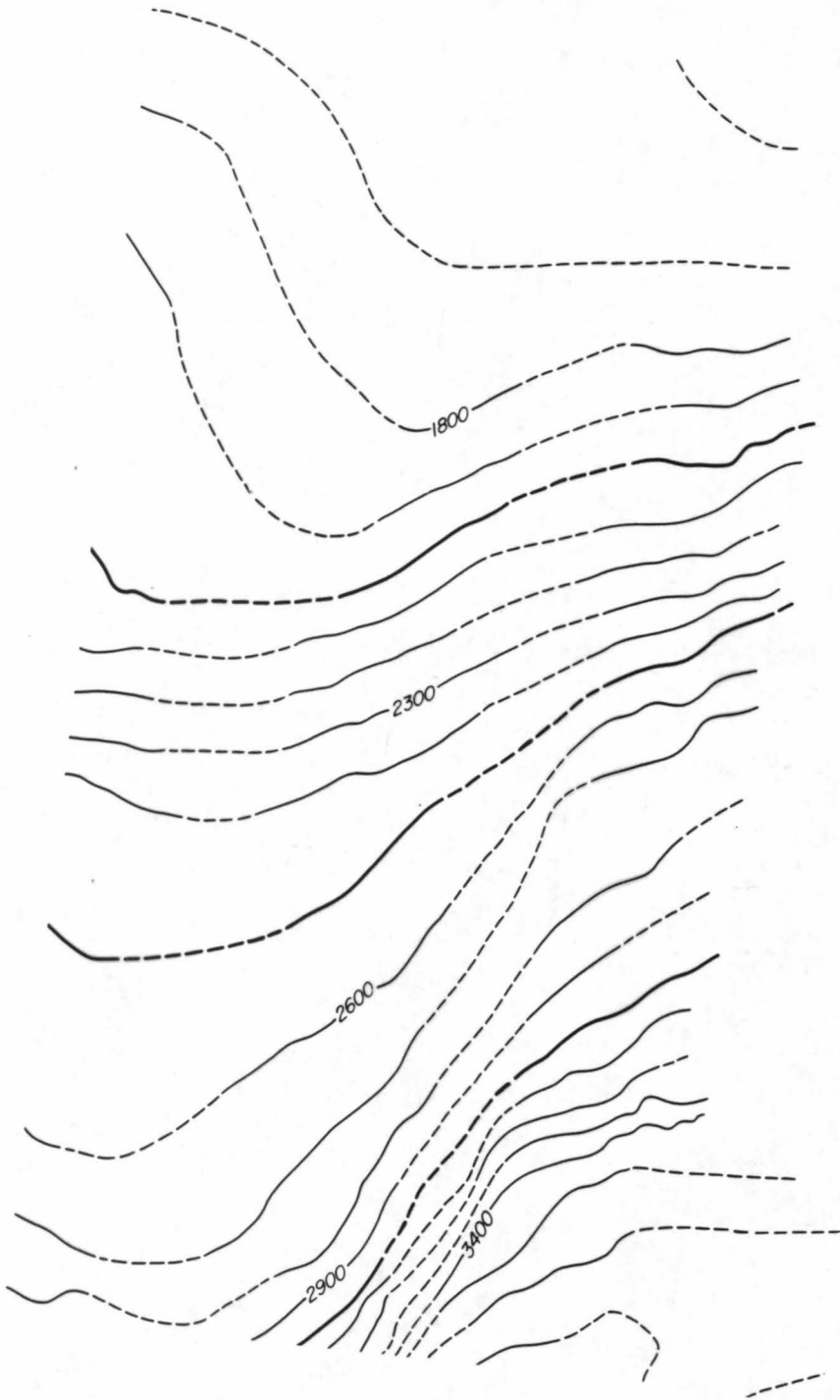
Debris Block

B

of about 200 square km. The slump can be recognized as a "horseshoe-shaped" feature bounded by dark debris channels on its margins and a sinuous scarp at its head (Figure 21a). Directly below the scarp is an intact portion, a large slump block that has rotated back, forming a large terrace that retains its original hemipelagic sediment cover, which appears light on the side-scan image (Figure 21a).

The most striking features in this sub-section are the numerous debris channels that lie along and within the slide feature. The edge of the slump is bounded by marginal shear channels, while the middle of the slump contains numerous parallel and anastomosing channels. These debris channels are dark on the side-scan, probably due to coarse debris within the channel. Similiar coarse debris in, and around the base of debris channels have been photographed on the submarine slopes of the Hawaiian Islands [Campbell, 1983; Tsutsui et al., 1986].

The classic lobate toe of this slump is imaged along a short N-S ship track (Figure 21a). Within this toe are dark circular features interpreted as debris blocks. Additional smaller head scarps are observed adjacent to the large slump on the southern mid-slope (Figure 21a, middle). These smaller slumps may be progressing up-slope, as indicated by the large over-flow channel which has a concentric shape similiar to the observed head scarps.

The large slump features indicate that the fore-arc is tilting while subsiding. Faulting observed on the multichannel records may behave as listric normal faults which intersect at depth, producing a shear-zone for decoupling and failure. Smaller slumps may be the cause of the terraced slope observed in the seismic profiles.

In contrast to the northern mid-slope where numerous kite-shaped knick points or erosional gullies are found, the southern mid-slope does not contain this type of channel.

Mid-slope basin area

The mid-slope basin lies in about 3800 m of water depth some 10-30 km from the trench axis (Figure 22). Light and dark areas in the basin represent small individual sub-basins (Figure 23b). These sub-basins are either flat lying (light) or slightly inclined and deformed (dark). Although the basin is a well developed structural basin, seismic profiles suggest a chaotic depositional history. Reflectors pinch-out and thin in various directions suggesting filling from different sides throughout the history of the basin. Large normal faults also offset the sediments and delineate the individual sub-basins [Hussong and Taylor, 1985]. These large faults have caused warping and tilting of the sediment fill, altering the original flat turbidite depositional surface.

These sub-basins seem to have responded differently to regional tectonic activity. The 3.5 kHz records show a sinusoidal warping of the layers of sediment (Figure 24b) and a slight incline of the whole surface (left hand side of Figure 24b and 24c). The side-scan image shows that on a scale of 10 km or so these sub-basin surfaces are affected by the warping and tilting and pass from a specular reflecting type to a backscattering type. One possible explanation for the change
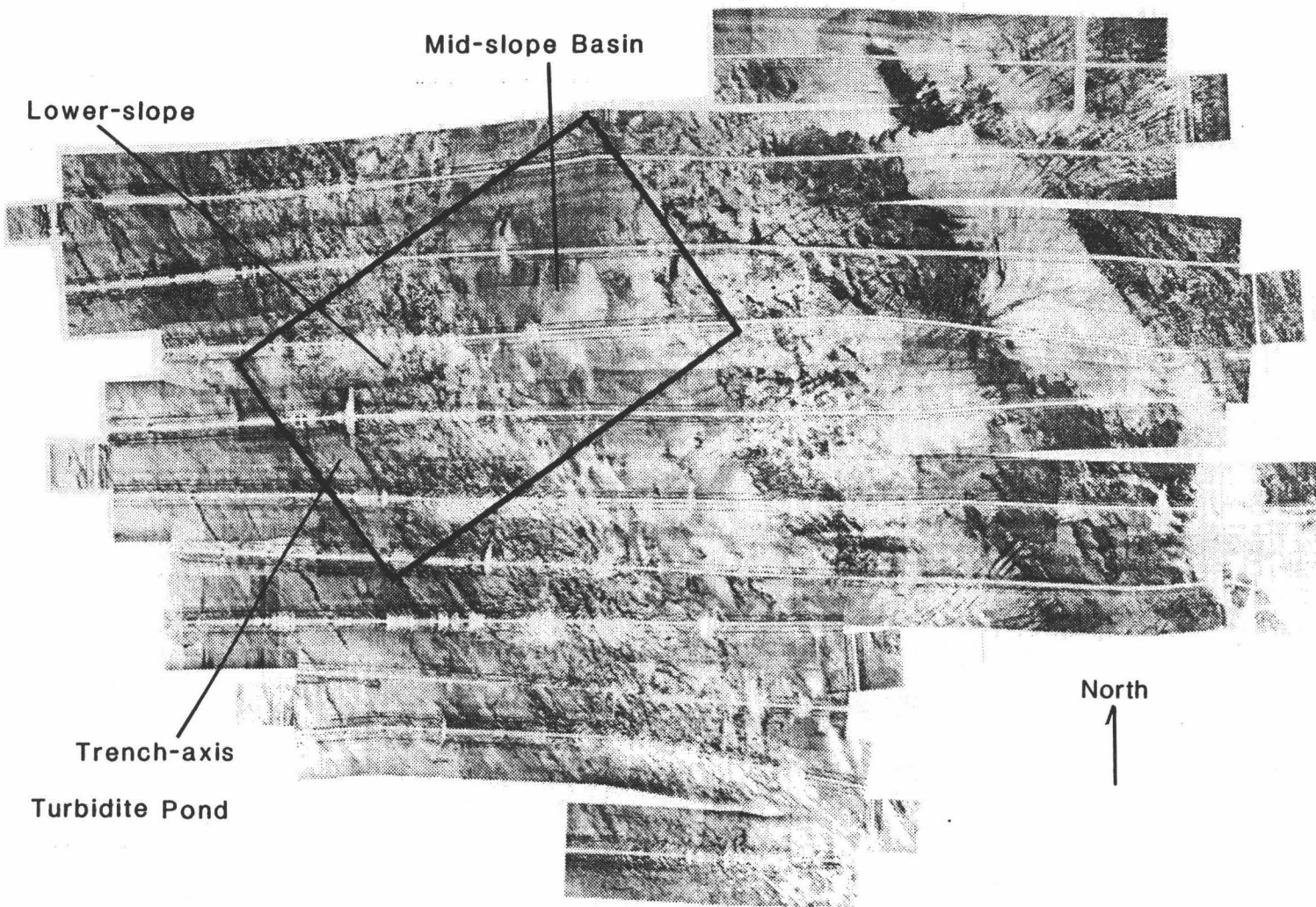
Fig. 22. Location of Figure 26 showing the mid-slope basin area, lower-slope (inner-trench wall), and trench-axis turbidite pond.

Plate VI. SeaMARC II bathymetry of the mid-slope basin area and the nearby trench, contoured at a 100 m interval. The lower-slope bathymetry shows a slope undisturbed by terraces and major conduits to the trench.

Fig. 23. a) SeaMARC II side-scan sonar mosaic of the mid-slope basin area, corresponding inner trench slope and trench axis. Along strike continuity of the accretionary packets can be traced across the swaths of the entire survey. Symmetrical features across the ship's track are data collection errors. b) Interpretive diagram of the area displaying features identified on the side-scan.

PLATE VI

Fig. 23 A

0 ─ 10KM

B

70
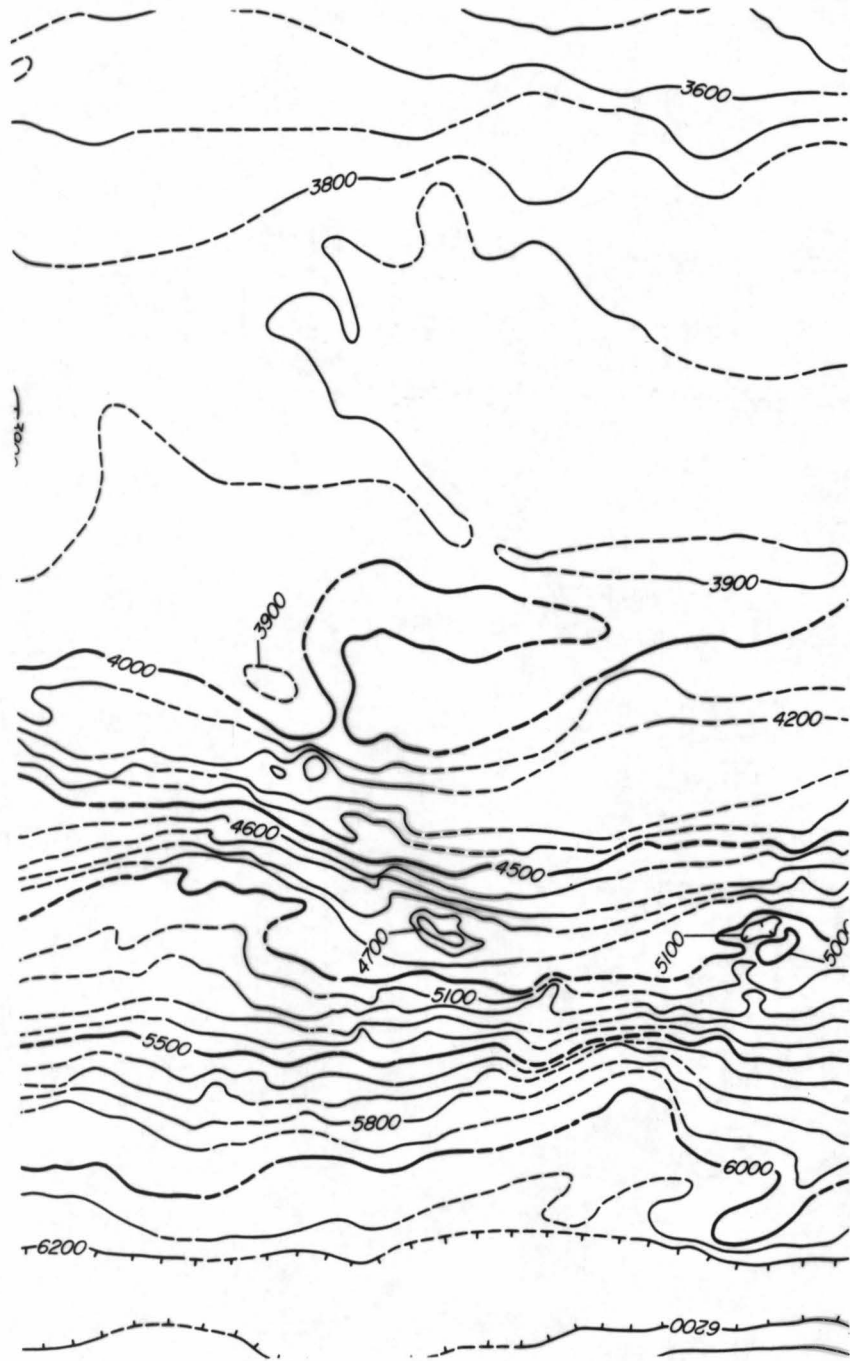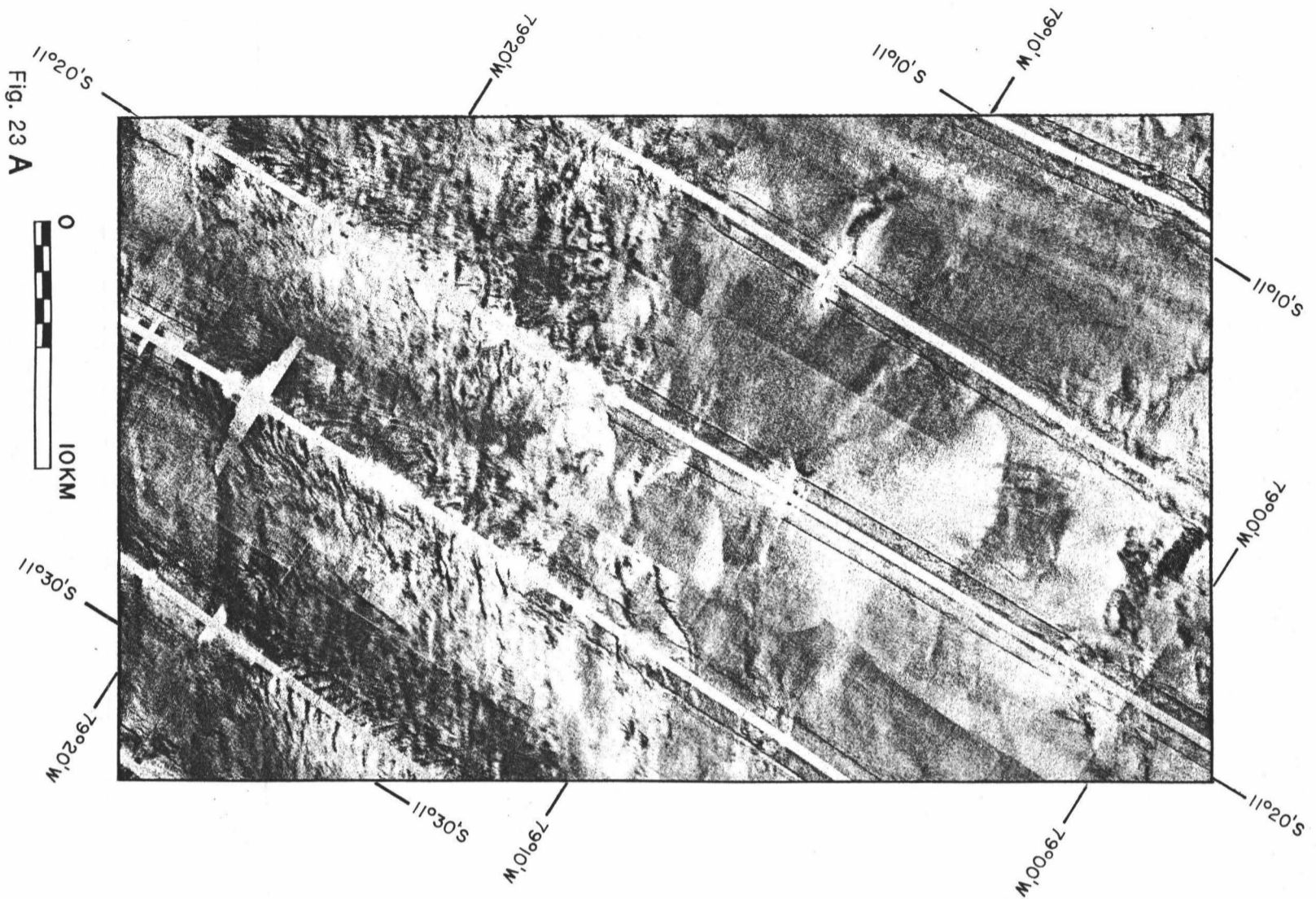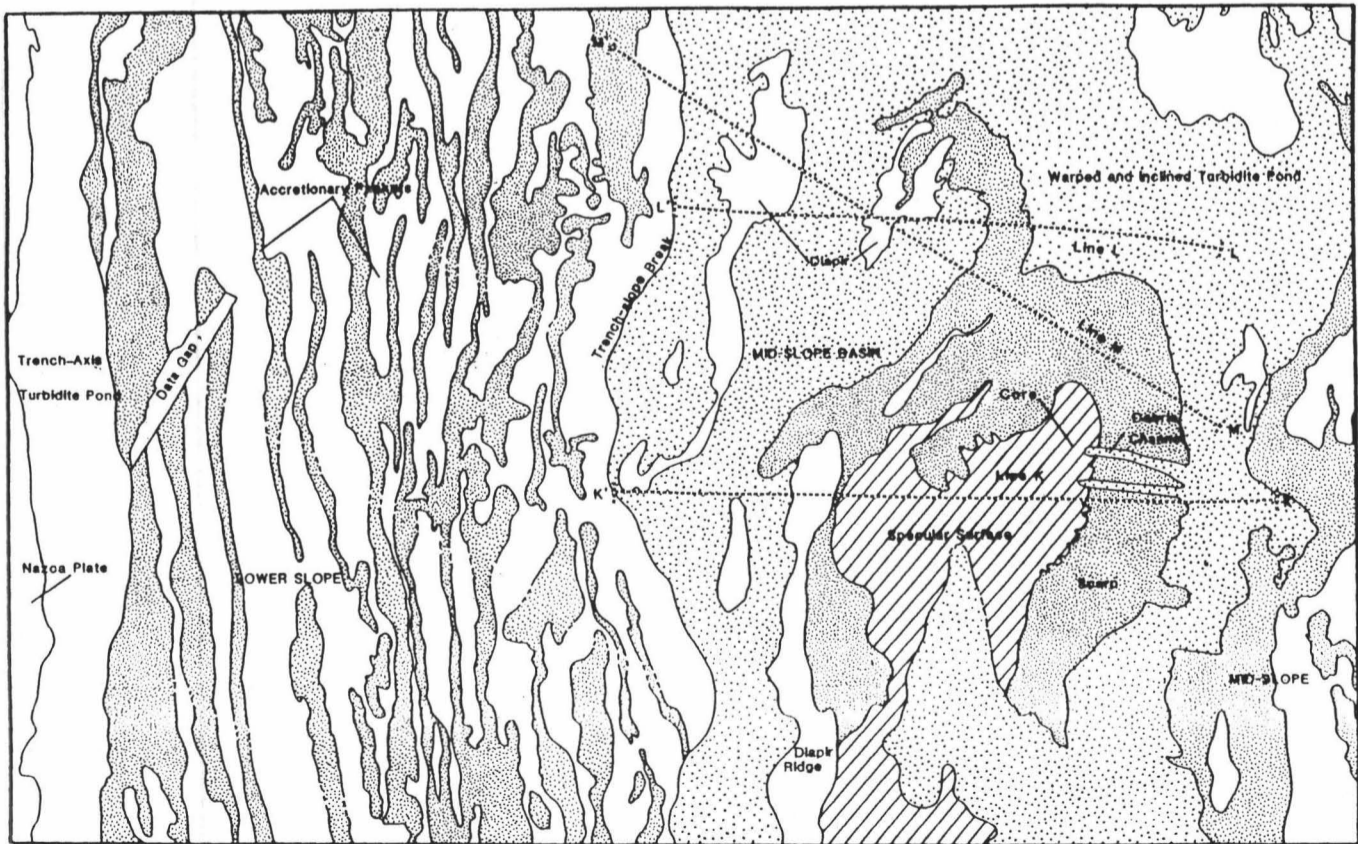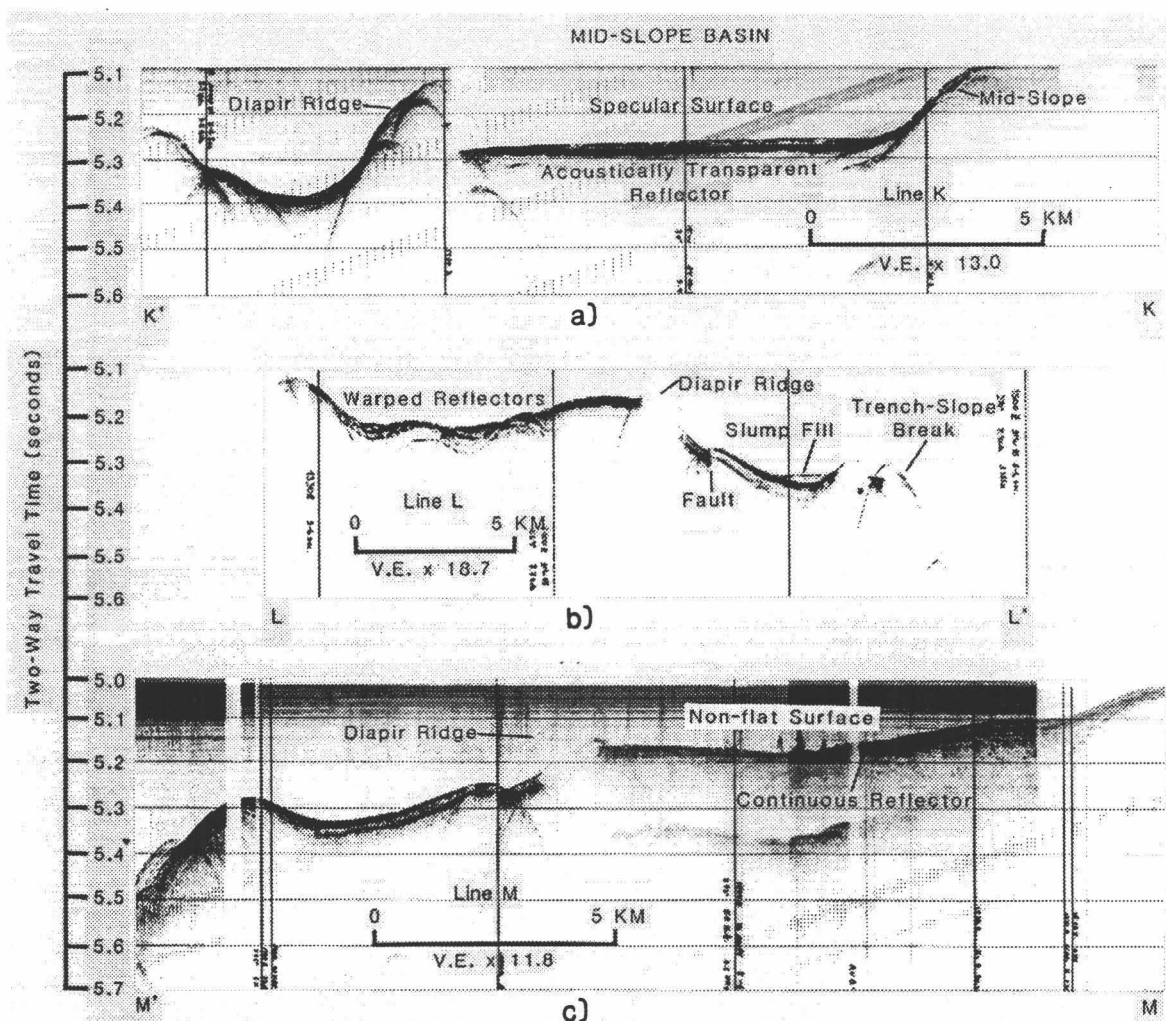
Fig. 24. Three 3.5 kHz seismic profiles across the mid-slope basin area. See Figure 23b for the exact line locations. These profiles help explain an interesting phenomenon that is seen on the side-scan (Figure 23a). The side-scan displays a light return in the area that Line K crosses. The lower two profiles (Line L and Line M) cross an adjacent area that displays a dark return. Both areas are fairly flat however the reflectors appear to differ between the profiles suggesting some difference in the surface of the sediment.

in echo character might be increased reflectivity as a result of compaction and dewatering of sediment caused by the warping.

A kasten core (WW7706-49) taken in this area at 3970 m water depth contained 204 cm of dark, olive-gray, siliceous, silty-clay size particles. The location of the core is shown on Figure 23b. The silty clay is described as firm and containing empty burrow holes throughout the length of the core. This core is located in one of the small turbidite basins which has a lighter color than surrounding basins on Figure 23a. The pond lies in 3945 m of water, and has an essentially flat, acoustically transparent surface (Figure 24a).

Another explanation might be subtle sediment features such as sediment ripples or scour marks which may cause changes in the sediment surface that in turn, may cause the different side-scan echo character [Bartlett et al., 1985].

Lower-slope

The lower-slope, also referred to as the inner-trench wall [Hussong and Taylor, 1985; Kulm et al., 1977], is outlined in Figure 23 and shown in profile in Figure 25. The lower-slope has a gradient ranging between 7° and 9°. Notable on the side-scan image is the across-track continuity of small shelves that are interpreted to be the surface expression of accreted imbricate sediment packets forming the

accretionary wedge. This accreted complex displays linear continuity for tens of kilometers along the lower-slope.

The accreted packets show little influences from sedimentation from up-slope sources. No ponds or up-slope channels can be seen. Apparently, therefore, these sediments are all uplifted from the trench axis, which was fed laterally from sediment sources outside the survey area.

Trench turbidite pond

The profile across the trench, shown in Figure 25, lies along 11° $15^{'}$ S. The trench depth is 6226 m and the width of the trench axis is about 3 km. The turbidite pond consists of about 400 m of sediments onlapping the Nazca Plate. The faint reflectors and rough topography, however make interpretation of the seismic stratigraphy difficult.

As suggested above, the sediment in the trench axis turbidite pond largely comes from lateral transport along the trench axis, presumably from the north where influx of sediment from terrestrial sources is higher with little sediment derived from the inner slope of the trench. Some sediment is derived from the Nazca plate where it flexes along the outer trench ridge prior to subduction under the Peru forearc [Prince et al., 1974].
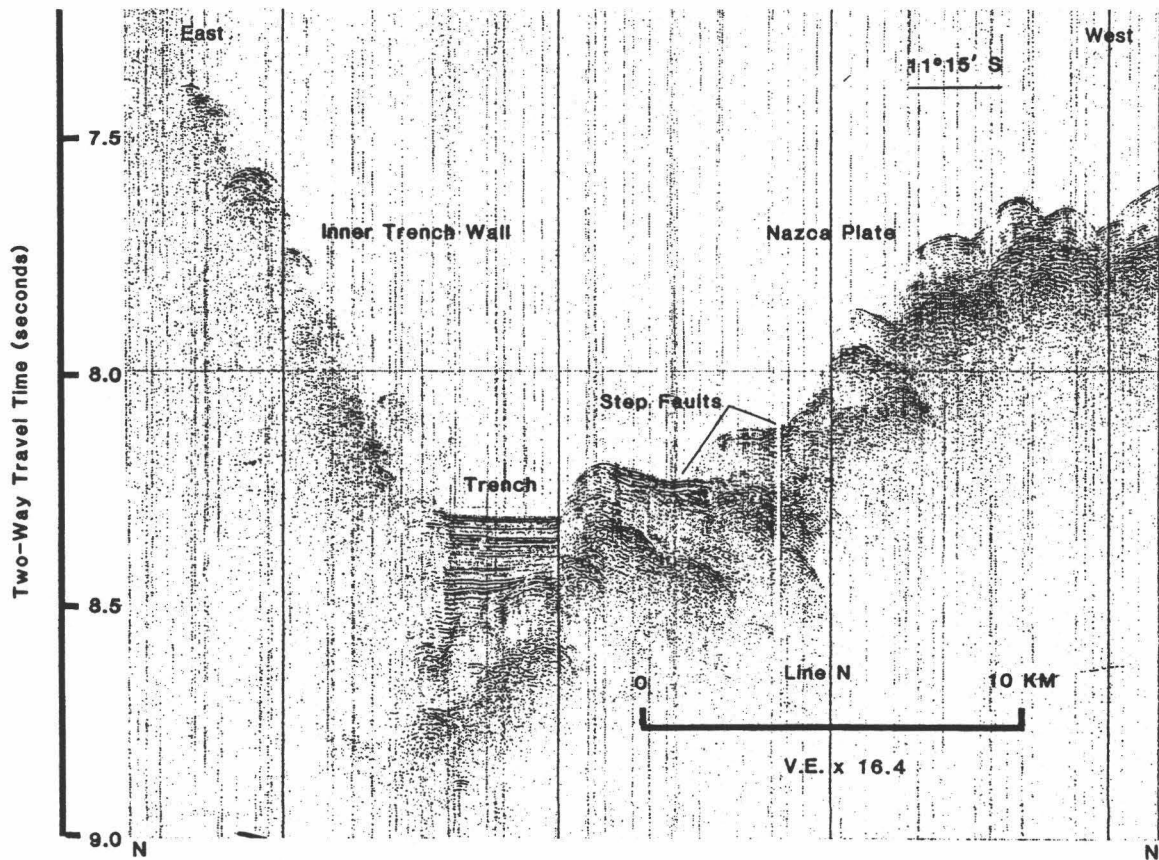
Fig. 25. A single-channel seismic profile (Line N) across the lower-slope (inner-trench wall), trench axis turbidite pond, and adjacent Nazca plate. See Figure 23b (N - N') for exact location of the line.

The main point is that the inner slope sediments primarily are derived from distant sources, not from sediment coming down from the adjacent fore-arc or slumping of the inner trench wall.

Chapter V

Summary and Conclusions

The fore-arc of the Peru convergent continental margin is believed to be subsiding, based on previous studies of benthic foraminifera and multichannel seismic reflection studies. Truncation of this continental margin due to tectonic erosion may cause this subsidence.

The Peru coastline adjacent to the fore-arc study area (11° – 12°S) is a desert which limits the amount of fluvial sediment that enters the ocean from the surrounding land. Instead, sedimentation along the submarine continental margin is mostly restricted to fine-grained biogenous material related to coastal upwelling and fine-grained eolian material. In most places this has left a thin veneer of unconformable hemipelagic sediment cover on the fore-arc. Underlying this unconsolidated sediment is a thick sequence of consolidated sediment and metasediment formed earlier in a fluctuating vertical tectonic environment.

Although this margin is considered to be an end-member of subduction tectonism, the lack of major terrestrial rivers, hemipelagic sedimentation due to coastal up-welling, and tectonic subsidence give this margin a unique morphology with respect to sedimentary features.

There are basically two different types of features that result from the subsidence of this margin; exclusively sediment deposition and

erosion forms and sedimentary structures that relate directly to the vertical tectonic movement of the fore-arc. SeaMARC II side-scan sonar and bathymetry provides a plan view of these sedimentary features. The sedimentalogical features are an order of magnitude smaller than previously described on this and other active margins. The distinctive character of the side-scan imagery on this fore-arc is determined in part by the sediment deposition and erosion features.

Sedimentary features related to structure are dominated by subsidence. Debris channels in the upper-slope maintain a preferred orientation, perpendicular to the trench, and are controlled by numerous normal faults in that direction. Extensional normal faulting has also formed a large graben that helps channel sediment down-slope. Other normal faulting is reflected in changes in gradients on adjacent large regional slopes and may be explained by a large fracture perpendicular to the trench. This large fracture bisects the survey area and possibly penetrates the fore-arc, allowing deep-seated fluids to escape and form mud-volcanoes. Other features related to tectonic activity include normal faulting parallel to the trench on the mid-slope which may cause large slides of consolidated sediment material.

In water depths shallower than 3800 m the fore-arc is distinctly lacking in an uniform cover of unconsolidated sediment. Only in places where it is flat and has a retaining structural high does the sediment remain trapped in pockets. The shallow turbidite pond dammed behind the mid-slope structural high is only a temporary accumulation of sediment. Local erosion and redeposition of sediment from this area of entrapment have created a unique set of anastomosing channels to form

an underwater "drainage network". These channels culminate into a main canyon that breaches the mid-slope structural high at a single location.

Channels on the mid-slope display straight paths, with no tributaries, which act as "avalanche shoots". When these channels encounter inflection points, called "knick-points", additional erosion occurs and may represent a lowering of the base-level. The final resting place for the transported sediment appears to be the mid-slope basin, where a thick sequence of sediment already has accumulated behind the lower-slope structural high.

These features characterize a morphologically and tectonically complex margin, and do not represent the currently accepted picture of active margin sedimentation. The Peru fore-arc area appears to be a margin dominated by erosion. The plan view of this fore-arc as seen on the SeaMARC II mosaic collected between 11° and 12° S latitude, reveals evidence of abundant tectonic activity. Surficial erosional features as evidenced in the SeaMARC II data seem to verify the older hypothesis that this fore-arc area is subsiding and eroding [Kulm et al., 1981b; Hussong and Wipperman, 1981]. Features that strike perpendicular to the trench are visible for the first time using SeaMARC II giving evidence of faulting and tectonic disruption perpendicular to the trench axis. Mass transportation of sediment down-slope to the mid-slope basin occurs through a unique series of channels that have formed from local erosion of the overlying sediment. The lower-slope structural high (trench-slope break) appears continuous and unbreached

along its length, and since major conduits have not formed for the transport of sediment down-slope into the trench, most of the sediment remains trapped above it.

References

Barazangi, M., and B. Isacks, Spatial Distribution of Earthquakes and Subduction of the Nazca plate beneath South America, Geology, 4, 686-692, 1976.

Bartlett, W. A., T. B. Reed IV, D. M. Hussong, Sediment Transport in the Peru Fore-arc (abstract), EOS Trans. AGU, 66, 1097, 1985.

Blackinton, J. G., D. M. Hussong, and J. Kosalos, First Results from a Combination of Side-scan Sonar and Seafloor Mapping System (SeaMARC II), Offshore Technology Conference, 4478, 307-311, 1983.

Blackinton, J. G., Bathymetric Mapping with SeaMARC II: An Elevation-Angle Measuring Side-scan Sonar System, Ph.D. Thesis, pp. 145, Univ. of Hawaii, Honolulu, May 1986.

Busch, W. H., and G. H. Keller, The Physical Properties of Peru-Chile Continental Sediments -- the Influence of Coastal Upwelling on Sediment Properties, J. Sed. Petro., 51, 705-719, 1981.

Busch, W. H., and G. H. Keller, Consolidation Characteristics of Sediments from the Peru-Chile Continental Margin and Implications for Past Sediment Instability, Marine Geology, 45, 17-39, 1982.

Busch, W. H., and G. H. Keller, Analysis of Sediment Stability on the Peru-Chile Continental Slope, Mar. Geotech., 5, 181-211, 1983.

Campbell, J. F., Hawaii Deep Water Cable Program Phase II, At-sea Route Survey, HIG Report 83-4, 50 pp., 1983.

Coulbourn, W. T., and R. Moberly, Structual Evidence of the Evolution of Fore-arc Basins off South America, Can. J. Earth Sci., 14, 102-116, 1977.

Dickinson, W. R., and D. R. Seely, Structure and Stratigraphy of Forearc Regions, AAPG Bull., 63, 2-31, 1979.

Hawkesworth, C. J., Isotope Characteristics of Magmas Erupted along Destructive plate Margins, in Andesites Orogenic Andesites and Related Rocks, edited by R. S. Thorpe, pp. 549-571, John Wiley & Sons, 1982.

Hilde, T. W. C., and G. F. Sharman, Fault Structure of the Descending plate and its Influence on the Subduction Process (abstract), EOS Trans. AGU, 59, 1182, 1978.

Howard, A. D., Drainage Analysis in Geologic Interpretation: A Summation, Am. Assoc. Pet. Geol. Bull., 51, 2246-2259, 1967.

Hussong, D. M., P. B. Edwards, S. H. Johnson, J. F. Campbell, and G. H. Sutton, Crustal structure of the Peru-Chile Trench: 8°- 12^OS Latitude, in The Geophysics of the Pacific Ocean Basin and its Margin, edited by G. H. Sutton, M. H. Manghnani, and R. Moberly, Geophys. Monogr. Am. Geophys. Union, 19, 71-86, 1976.

Hussong, D. M., and L. K. Wipperman, Vertical Movement and Tectonic Erosion of the Wall of the Peru-Chile Trench near 11^O30' S latitude, Geol. Soc. Am. Mem., 154, 509-524, 1981.

Hussong, D. M., and P. Fryer, Back-arc Seamounts and the SeaMARC II Seafloor Mapping System, EOS Trans. AGU, 64, 627-632, 1983.

Hussong, D. M., Mud Volcanoes, in Yearbook of Science and Technology 1986, pp. 286-289, McGraw-Hill, New York, 1985.

Hussong, D. M., T. B. Reed, W. A. Bartlett, K. L. Mansfield, B. Taylor, T. W. C. Hilde, and L. W. Kulm, SeaMARC II Survey of the Peru Trench and Continental Margin (abstract), EOS Trans. AGU, 66, 377, 1985.

Hussong, D. M., and B. Taylor, Peru Fore-arc Structure and Tectonic Disruption (abstract), EOS Trans. AGU, 66, 1096, 1985.

James, D. E., Subduction of the Nazca plate beneath Central Peru, Geology, 6, 174-178, 1978.

Johnson, A. M., The Climate of Peru, Bolivia and Ecuador, in <u>Climates of Central and South America</u>, edited by W. Schwerdtfeger, pp. 147-218, Elsevier, New York, 1976.

Krissek, L. A., K. F. Scheidegger, and L. D. Kulm, Surface Sediments of the Peru-Chile Continental Margin and the Nazca plate, <u>Geol. Soc. Am. Bull.</u>, <u>91</u>, 321-331, 1980.

Kulm, L. D., W. J. Schweller, and A. Masais, A Preliminary Analysis of the Subduction Processes along the Andean Continental Margin, 6° to 45^OS, in <u>Island Arcs Deep Sea Trenches and Back-arc Basins</u>, edited by M. Talwani and W. C. Pitman III, 285-301, Amer. Geophys. Union, Marice Ewing Symposium, Series I, 1977.

Kulm, L. D., J. Dymond, E. J. Dasch, and D. M. Hussong (Eds.), <u>Nazca plate: Crustal Formation and Andean Convergence</u>, 824 pp., Geol. Soc. Am. Mem., 154, 1981a.

Kulm, L. D., H. Schrader, J. M. Resig, T. M. Thornburg, A. Masais, and L. Johnson, Late Cenozoic Carbonates on the Peru Continental Margin: Lithostratigraphy, Biostratigraphy, and Tectonic History, <u>Geol. Soc. Am. Mem.</u>, <u>154</u>, 469-508, 1981b.

Kulm, L. D., J. M. Resig, T. M. Thornburg, and H. J. Schrader, Cenozoic Structure, Stratigraphy and Tectonics of the Central Peru Forearc,

in Trench-forearc Geology: Sedimentation and Tectonics on Modern an
Ancient Active Plate Margins, edited by J. K. Leggett, 151-169,
Geol. Soc. Sp. Pub. No. 10, Blackwell Scientific Publications,
Oxford, England, 1982.

Kulm, L. D., E. Suess, and T. M. Thornburg, Dolomites in Organic-rich
muds of the Peru Fore-arc Basins: Analogue to the Monterey
Formation, in Dolomites of the Monterey Formation and Other Organic-
Rich Units, edited by R. E. Garrison, et al., pp. 29-47, Pacific
Section S.E.P.M., 1984.

Kulm, L. D., T. Thornburg, E. Suess, D. M. Hussong, Basement Framework
Lithologies and Tectonics of the Truncated Central Peru Fore-arc
(abstract), EOS Trans. AGU, 66, 1096, 1985.

Kulm, L. D., E. Suess, T. M. Thornburg, R. W. Embley, D. M. Hussong,
and J. M. Resig, Fluid enting Processes and their Relation to
Tectonic Styles in Subduction Zones of the Eastern Pacific
(abstract), Intl. Kaiko Conference, 28, 1986.

Masias, J. A., Morphology, Shallow Structure, and Evolution of the
Peruvian Continental Margin, 6° to 18° S, M. S. Thesis, Corvallis,
Oregon State University, 92 pp., 1976.

Mazel, C., Side-scan Sonar Training Manual, 144 pp., Klein Associates, Inc., New Hampshire, 1985.

Peake, W. H., and T. L. Oliver, The Response of Terrestrial Surfaces at Microwave Frequencies, Ohio State University Electroscience Lab., 2440-7, Tech. Rep. AFAL-TR-70-301, Columbus, Ohio, 1971.

Pearce, J. A., Trace Element Characteristics of Lavas from Destructive Plate Boundaries, in Andesites Orogenic Andesites and Related Rocks, edited by R. s. Thorpe, 525-548, John Wiley & Sons, 1982.

Prince, R. A., Resig, J. M., L. D. Kulm, and T. C. Moore, Jr., Uplifted Turbidite Basins on the Seaward wall of the Peru Trench, Geology, 2, 607-611, 1974.

Reed IV, T. B., Digital Image Processing and Quantitative Analysis of SeaMARC II Side-scan Sonar Imagery, Ph.D. Dissertation, Univ. of Hawaii, 256 pp., 1987.

Sabins, F. F., Jr., Remote Sensing Principles and Interpretations, 426 pp., W. H. Freeman and Co., San Francisco, 1978.

Schweller, W. J., and L. D. Kulm, Depositional Patterns and Channelized Sedimentation in Active Eastern Pacific Trenches, in Sedimentation in Submarine Canyons, Fans, and Trenches, edited by D. J. Stanley

and G. Kelling, pp. 311-324, Dowen, Hutchinson and Ross, Inc., Stroudsburg, Pennsylvania, 1978.

Searle, R. C., T. J. G. Francis, T. W. C. Hilde, M. L. Somers, J. Revie, C. L. Jacobs, M. R. Saunders, B. J. Barrow, and S. V. Bickwell, 'Gloria' Side-scan Sonar in the East Pacific, EOS Trans. AGU, 62, 121-122, 1981.

Sutton, G. H., M. H. Manghnani, and R. Moberly (Eds.), The Geophysics of the Pacific Ocean Basin and Its Margin, 480 pp., AGU Geophysical Monograph, 19, Washington D. C., 1976.

Thornburg, T., and L. D. Kulm, Sedimentary Basins of the Peru Continental Margin: Structure, Stratigraphy, and Cenozoic Tectonics from 6°S to 16°S latitude, Geol. Soc. Am. Mem., 154, 393-422, 1981.

Thorpe, R. S. and Francis, P. W., Variations in Andean Andesite Compositions and their Petrogenetic Significance, Tectonophysics, 57,53-70, 1979.

Trabant, P. K., Applied High-resolution Geophysical Methods, 265 pp., IHRDC, Boston, 1984.

Tsutsui, B., J. F. Campbell, and W. T. Coulbourn, Storm Generated, Episodic Sediment Movements off Kahe Point, Oahu, Hawaii, <u>Marine Geology</u>, (in press), 1986.

von Huene, R., L. D. Kulm, and J. Miller, Structure of the Frontal Part of the Andean Convergent Margin, <u>J. Geophys. Res.</u>, <u>90</u>, 5429-5442, 1985.

Westbrook, G. K., and M. J. Smith, Long Decollements and Mud Volcanoes: Evidence from the Barbados Ridge Complex for the Role of High Pore-Fluid Pressure in the Development of an Accretionary Complex, <u>Geology</u>, <u>11</u>, 279-283, 1983.

DATE DUE

JUL 13 1988			
AUG 18 1988			
DEC 16 1988			
JAN 6 1988			
AR 24 1989			
MAY 05 1989			
OC 4 1989			
APR 3 1990			